

本次查收引工作是根据委托人提供的作者姓名、组织机构及文献列表进行的, 委托人信息如下:

作者姓名: 白俊毅

作者单位: 成都肛肠专科医院

检索范围:

- 科学引文索引 (Science Citation Index Expanded): 1900年-2024年
- 期刊引证报告 (Journal Citation Reports): 1997年-2022年
- 中科院期刊分区表: 2005年-2022年

检索结果:

检索类型	数据库	年份范围	记录数	第一作者
SCI-E 收录	SCI-EXPANDED	2022	1	1

附件一: SCI-E 收录

#	作者	作者顺序	检索作者地址	标题	来源出版物	JCR影响因子	JCR分区	中科院分区	文献类型	入藏号
1	Bai, JY; Xiong, TT; Wang, X; Cheng, YF; Luo, RF; Yang, XD; Fu, CM	第一作者	Chengdu Univ Tradit Chinese Med, Pharm Sch, State Key Lab Southwestern Chinese Med Resources, Chengdu, Peoples R China.	Potential mechanisms of Lian-Zhi-Fan solution for TNBS-induced ulcerative colitis in rats via a metabolomics approach	FRONTIER S IN PHARMACOLOGY 2022, 13: 1014117.	• 5.988 (2021);	• PHARMACOLOGY & PHARMACY [Q1] (2021);	• 小类(升级版)(2021)药 学 [2区]; • 大类(升级版)(2021)医 学 [2区] Top 期刊;	J Article	WOS:000 89878710 0001

合计

1

第 1 条, 共 1 条:

标题: Potential mechanisms of Lian-Zhi-Fan solution for TNBS-induced ulcerative colitis in rats via a metabolomics approach

作者: Bai, JY (Bai, Junyi); Xiong, TT (Xiong, Tingting); Wang, X (Wang, Xiao); Cheng, YF (Cheng, Yanfen); Luo, RF (Luo, Ruifeng); Yang, XD (Yang, Xiangdong); Fu, CM (Fu, Chaomei)

来源出版物: FRONTIERS IN PHARMACOLOGY 卷: 13 文献号: 1014117 出版年: DEC 2 2022

入藏号: WOS:000898787100001 PubMed ID: 36532763

文献类型: Article 出版物类型: J

作者地址: [Bai, Junyi; Wang, Xiao; Cheng, Yanfen; Luo, Ruifeng; Fu, Chaomei] Chengdu Univ Tradit Chinese Med, Pharm Sch, State Key Lab Southwestern Chinese Med Resources, Chengdu, Peoples R China.; [Bai, Junyi; Yang, Xiangdong] Chengdu Anorectal Hosp, Chengdu, Peoples R China.; [Xiong, Tingting] Sichuan Prov Matern & Child Hlth Care Hosp, Chengdu, Peoples R China.

通讯作者地址: Fu, CM (通讯作者), Chengdu Univ Tradit Chinese Med, Pharm Sch, State Key Lab Southwestern Chinese Med Resources, Chengdu, Peoples R China.; Yang, XD (通讯作者), Chengdu Anorectal Hosp, Chengdu, Peoples R China.





OPEN ACCESS

EDITED BY

Hongxun Tao,
Jiangsu University, China

REVIEWED BY

Chao Ai,
Guangdong Ocean University, China
JingJing Li,
Hong Kong Polytechnic University,
Hong Kong SAR, China
Zhangfeng Zhong,
University of Macau, China

*CORRESPONDENCE

Xiangdong Yang,
936430462@qq.com
Chaomei Fu,
chaomeifu@126.com

SPECIALTY SECTION

This article was submitted
to Ethnopharmacology,
a section of the journal
Frontiers in Pharmacology

RECEIVED 08 August 2022

ACCEPTED 16 November 2022

PUBLISHED 02 December 2022

CITATION

Bai J, Xiong T, Wang X, Cheng Y, Luo R,
Yang X and Fu C (2022), Potential
mechanisms of Lian-Zhi-Fan solution
for TNBS-induced ulcerative colitis in
rats *via* a metabolomics approach.
Front. Pharmacol. 13:1014117.
doi: 10.3389/fphar.2022.1014117

COPYRIGHT

© 2022 Bai, Xiong, Wang, Cheng, Luo,
Yang and Fu. This is an open-access
article distributed under the terms of the
[Creative Commons Attribution License
\(CC BY\)](https://creativecommons.org/licenses/by/4.0/). The use, distribution or
reproduction in other forums is
permitted, provided the original
author(s) and the copyright owner(s) are
credited and that the original
publication in this journal is cited, in
accordance with accepted academic
practice. No use, distribution or
reproduction is permitted which does
not comply with these terms.

Potential mechanisms of Lian-Zhi-Fan solution for TNBS-induced ulcerative colitis in rats *via* a metabolomics approach

Junyi Bai^{1,2}, Tingting Xiong³, Xiao Wang¹, Yanfen Cheng¹,
Ruifeng Luo¹, Xiangdong Yang^{2*} and Chaomei Fu^{1*}

¹State Key Laboratory of Southwestern Chinese Medicine Resources, Pharmacy School, Chengdu University of Traditional Chinese Medicine, Chengdu, China, ²Chengdu Anorectal Hospital, Chengdu, China, ³Sichuan Provincial Maternity and Child Health Care Hospital, Chengdu, China

Lian-Zhi-Fan (LZF) decoction is a hospital-prescribed traditional Chinese medicine botanical drug prepared by the fermentation of decocted Coptidis Rhizome (Huanglian), Gardeniae Fructus (Zhizi), and alum (Baifan). It has been used clinically in China for the treatment of anal fistula, perianal abscess, ulcerative colitis (UC), and other anorectal diseases for hundreds of years. However, due to the complexity of traditional Chinese medicine, the potential mechanisms of LZF in the treatment of UC have remained unknown. This study primarily investigated the remarkable pharmacological effects of LZF on TNBS-induced UC rats. To explore the complex targets and regulatory mechanisms of metabolic networks under LZF intervention, a metabolomics approach mediated by HPLC/Q-TOF-MS analysis was used to screen the different metabolites and their metabolic pathways in the serum in order to characterize the possible anti-UC mechanisms of LZF. After rectal administration of LZF for seven consecutive days, significant amelioration effects on body weight loss, DAI score, and colon inflammation were found in UC rats. Based on this, further metabolomics identified 14 potential biomarkers in the treatment of UC with LZF, of which five possessed diagnostic significance: L-alanine, taurocholic acid, niacinamide, cholic acid, and L-valine. These metabolites are mainly involved in 12 metabolic pathways, including nicotinate and nicotinamide metabolism, glycospholipid metabolism, arginine and proline metabolism, primary bile acid biosynthesis, and pantothenate and CoA biosynthesis. These metabolic pathways suggest that LZF ameliorates UC by regulating amino acid metabolism, fat metabolism, and energy production. This study provides a useful approach for exploring the potential mechanisms of herbal prescription in UC treatment mediated by metabolomics.

KEYWORDS

ulcerative colitis, metabolomics, HPLC/Q-TOF-MS, TNBS, rectal administration

1 Introduction

Ulcerative colitis (UC) is a nonspecific inflammatory disease, with persistent or recurrent abdominal pain, diarrhea, and purulent mucinous bloody stool as its main clinical manifestations. It can extend from the rectum to the proximal colon, and it is one of the chronic inflammatory bowel diseases (IBDs) (Ungaro et al., 2017). UC has the characteristics of early onset, easy recurrence, long course of disease, and increased cancer risk, resulting in poor quality of life and high economic burden (Hoivik et al., 2013). In recent years, the incidence rate of UC has been high in developed countries but has tended to be stable. Moreover, it has been increasing year by year in developing countries. Therefore, UC has become a refractory disease worldwide (Alatab et al., 2020). The exact pathogenesis of UC is not completely clear, but it is related to immune disorder, intestinal microbiota imbalance, genetic susceptibility, environment, and other factors (Kobayashi et al., 2020). At present, drug-graded treatment is often implemented in clinic, according to the severity of UC: 5-aminosalicylic acid is selected as the first-line drug in mild and moderate cases and immunosuppressive or biological drugs in moderate and severe cases. In addition, corticosteroids and fecal transplantation can be used to treat acute UC. However, these treatments have limited efficacy and obvious side effects. Therefore, the use of alternative therapies with high efficiency and low side effects in traditional Chinese medicine (TCM) has been a breakthrough in UC treatment and has attracted extensive attention (Zhang et al., 2013; He et al., 2022).

Lian-Zhi-Fan (LZF) decoction (z20080191) is a hospital-grade preparation used at Chengdu Anorectal Hospital. It is a liquid prepared from the fermentation of *Coptidis Rhizome* (Huanglian), *Gardeniae Fructus* (Zhizi), and alum (Baifan). In China, it has been used for hundreds of years because of its remarkable clinical effects. It is commonly used in the prevention and treatment of anorectal diseases such as anal fistula, anal condyloma acuminatum, anal dilatation, perianal abscess, and chronic ulcerative proctitis. LZF contains a variety of effective components for the treatment of UC, including berberine, coptisine, gardenoside, and genipin. Berberine, the representative component of *Coptidis Rhizome*, could effectively improve UC by reducing inflammation, regulating immunity, regulating the intestinal flora, and protecting the intestinal barrier (Li et al., 2016; Li et al., 2020; Liao et al., 2020). Geniposide, a representative component of *Gardeniae Fructus*, could improve DSS-induced UC by inhibiting oxidative stress, reducing inflammation, and protecting the intestinal barrier (Zhang et al., 2017; Yang et al., 2020; Lu et al., 2021). Deepening research into the mechanism of the compounds contained in LZF for improving UC has revealed the mechanism of LZF as an effective therapeutic for UC to a certain extent. However, in view of this complex formulation, there is no detailed study of the mechanism of action of LZF in improving UC.

Metabolomics reflects the relationship between the state of the biological system and the concentration of small-molecule metabolites, and it characterizes the overall metabolic spectrum in complex biological matrixes. It is especially suitable for characterizing the mechanism of action of a variety of stimulating factors on the whole body. Therefore, it is increasingly used to study the mechanism of TCM in improving diseases (Wang et al., 2017; Wang et al., 2019). Metabolomics was used to find that Xiaokeyinshui extract combination improves the symptoms of Type 2 diabetes mellitus mice by regulating glucose metabolism, lipid metabolism, and amino acid metabolism (Xiang et al., 2021). Metabolomics has shown that Huang-Lian-Jie-Du decoction reduces acute UC in mice by regulating arachidonic acid metabolism and glycerophospholipid metabolism (Yuan et al., 2020). Metabolomics technology was also used to discover and study changes in 36 potential biomarkers upon compound sophorae decoction treatment in UC rats, revealing the mechanism of this prescription in improving UC (Hong et al., 2021). Obviously, the wide application of metabolomics technology has provided a new perspective for the study of the mechanism of action of TCM.

In this study, the improvement effects of LZF on TNBS-induced UC in rats was studied based on the metabolomics of HPLC/Q-TOF-MS. The anti-colitis effect of LZF was evaluated by colon length, body weight change, DAI, and H&E pathological sections. Metabolomic analysis was performed on serum samples of rats to screen potential marker metabolites and evaluate their clinical diagnostic value, enrich metabolic pathways, and reveal the mechanism of LZF in improving UC from a metabolic perspective.

2 Materials and methods

2.1 Chemicals and animal

TNBS (5%) was purchased from Sigma-Aldrich (United States). LZF was purchased from Chengdu Anorectal Hospital (Chengdu, China). Ethanol was purchased from Chengdu Kelong Chemical Reagent Factory (Chengdu, China). Paraformaldehyde was purchased from Sigma-Aldrich (United States). Sodium chloride injection was obtained from Sichuan Kelun Pharmaceutical Co., Ltd. (Chengdu, China).

Male Sprague-Dawley rats (180–200 g) were obtained from Chengdu Dossy Biological Technology Co., Ltd. (Chengdu, China). The rats were housed under standard conditions (temperature 20–23°C, humidity 50 ± 10%, 12 h light/dark cycles) and supplied *ad libitum* with food and distilled water. All animal studies were conducted and performed as per the protocol approved by the Animal Welfare Committee of Chengdu University of Traditional Chinese Medicine.

2.2 Composition of LZF solution

The LZF solution (1000 ml) was prepared by fermentation and filtration of 43.5 g *Coptis chinensis* Franch [*Ranunculaceae*; *Coptidis Rhizoma*], 31.5 g *Gardenia jasminoides* J. Ellis [*Rubiaceae*; *Gardeniae Fructus*], and 4.35 g alum [$KAl(SO_4)_2 \cdot 12H_2O$].

2.3 Preparation of LZF solution

LZF was prepared according to the standard of LZF solution (approved by Sichuan Food and Drug Administrations, zbz20080900). Huanglian (43.5 g) and Zhizi (31.5 g) were crushed, soaked in water for 24 h, and decocted three times. The same amount of alum was added during each decocting, with a total of 4.35 g added. In the first decocting, eight times the amount of water was added and decocted for 45 min. In the second and third decoctions, six times the amount of water was added and decocted for 30 min. The decoctions were combined and concentrated to 1000 ml and placed at room temperature for fermentation for three weeks, then filtered to obtain LZF.

2.4 Animal treatment

The SD rats were randomly divided into four groups (six rats in each group): the control group, model group, LZF-L group, and LZF-H group. After adaptive feeding, the rats in the control group were given 2 ml of 0.9% normal saline through the rectum, and rats in other groups were given TNBS-solution (30 mg/kg, soluble in 50% ethanol) inserted to 8 cm from the anus to induce UC (Yang et al., 2017). After successful modeling, the rats in the control and model groups were rectally given 2 ml normal saline, the rats in the LZF-L group were rectally given LZF (0.4 g/kg, crude botanical drug), and the rats in LZF-H group were rectally given LZF solution (0.8 g/kg, crude botanical drug). All groups were rectally given the corresponding solutions continuously for seven days. During the whole experiment, the body weight and disease activity index (DAI) score were recorded daily. DAI was calculated as the sum of weight loss (0 = <5%, 1 = 5–10%, 2 = 10–15%, 3 = 15–20%, and 4 >20%); fecal bleeding (0 = none, 1 = mild occult blood, 2 = severe occult blood, 3 = visible blood, and 4 = major bleeding); and stool consistency status (0 = normal, 1 = soft, 2 = loose stools, 3 = diarrhea, and 4 = severe diarrhea) (Zhang et al., 2022a; Zhang et al., 2022b).

2.5 Sample collection and preparation

After fasting for 24 h following the final administration, the rats were anesthetized with sodium pentobarbital, and their blood was collected from the abdominal aorta. Colon tissue was obtained by dissection, and the length was measured.

After the blood was coagulated at 4°C for 2 h, it was centrifuged at 3500 rpm for 10 min, and its supernatant was transferred to a centrifuge tube and immediately stored at –80°C until analysis.

2.6 Histological evaluation

After colon tissue was fixed with 10% formalin, it was embedded in paraffin, cut into 5- μ m sections, and stained with hematoxylin and eosin (H&E) (Wang et al., 2021). Images were collected using an optical microscope.

2.7 Metabolic analysis of serum samples

2.7.1 Preparation of serum samples

Serum samples were thawed at 4°C, and 100 μ L sample was put into a centrifuge tube with 400 μ L of methanol, vortexed for 60 min, and centrifuged at 12,000 rpm for 10 min at 4°C. The supernatant was filtered through a 0.22- μ m membrane and analyzed by HPLC/Q-TOF-MS.

A volume of 20 μ L of each sample was removed and mixed to obtain a quality control sample to eliminate systematic errors in the experiment.

2.7.2 HPLC/Q-TOF-MS conditions

All analyses were carried out on the Agilent 1200 HPLC instrument (Agilent, Germany). The chromatographic separation was performed on an ACE Excel C18 column (100 mm \times 2.1 mm, 3.0 mm) at 40°C. The mobile phases were composed of (A) 0.1% (v/v) formic acid aqueous solution and (B) acetonitrile containing 0.1% formic acid with a flow rate of 0.4 ml/min. The gradient elution program for serum samples was carried out as follows: 0–2 min, 5% B; 2–7 min, 5–65% B; 7–20 min, 65–95% B; 20–22 min, 95% B; 22–23 min, 95–5% B; and 23–28 min, 5% B. The sample injection volume was set to 3 μ L.

Mass spectrometry analysis was conducted to confirm the peak identities using the Agilent 6530 Q-TOF mass spectrometer (Agilent Corp, United States) coupled with an electrospray ionization (ESI) source. MassHunter Workstation software (Agilent Technologies, United States) was employed for the system operation. The operation conditions of the mass spectrometer were as follows: capillary voltage of 4.0 kV for the positive ion mode and 3.5 kV for the negative ion mode; nebulizer pressure of 35 psig; gas temperature of 320°C; gas flow of 12 L/min; collision energy of 35 eV; drying gas temperature of 300°C; and drying gas flow rate of 6 L/min. The mass range was set from 50 to 1100 Da with the full scan mode.

2.7.3 Data processing and multivariate analysis

The initial HPLC/Q-TOF-MS data were pre-processed with Peak Picking and Threshold Peak Filer in MSConvert (version

3.0, ProteoWizard, United States) to generate mzXML documents. Then the document was imported into XCMS website software (<https://xcmsonline.scripps.edu>) for noise removal, baseline correction, and peak alignment and to automatically generate a TSV document with a multi-dimensional data matrix composed of retention time, peak intensity, and mass-to-charge ratio (m/z). The final peak areas in the TSV files were re-obtained using the 80% correction method.

The pre-treatment data files were imported into the SIMCA (ver. 14.0) software package (Umetrics, Umea, Sweden) for multivariate statistical analyses including PCA, PLS-DA, and OPLS-DA. Differences between groups were explored based on endogenous metabolites, and variable importance in projection (VIP) values >1.5 were selected to prove the contributions to variation (Sun et al., 2018). These differential metabolites were considered as potential chemical markers. Then they were further identified via GraphPad Prism software (version 9.0, GraphPad, United States) and analyzed with a one-way ANOVA test to evaluate significant differences between the groups ($p < 0.05$).

2.7.4 Biomarker identification and pathway analysis

The screening of potential metabolites was based on the retention time, the accurate quality of MS and MS/MS, and the results of comparison against various databases, such as the Human Metabolome Database (<http://www.hmdb.ca>) and the Kyoto Encyclopedia of Genes and Genomes (<http://www.genome.jp/kegg/>). Various metabolic pathways of biomarkers were further analyzed via the MetaboAnalyst database (<http://www.metaboanalyst.ca/>) to obtain the enrichment analysis and biological functions of different metabolites.

2.8 Statistical analysis

Data were presented as mean \pm SD. Statistical comparisons were assessed by one-way ANOVA test between different groups using GraphPad Prism (version 9.0, GraphPad, United States). Values of $*p < 0.05$ were regarded as indicating significant differences.

3 Results

3.1 Therapeutic effects of LZF on UC rats

The clinical symptoms of UC often include diarrhea, bloody stool, and weight loss. Grading the severity of these three items to form the DAI score has become an important index in drug treatment of colitis (Wang et al., 2021). In addition, colon length intuitively reflects the degree of colon lesions, which are important detection indicators (Yu T et al., 2021). As shown

in Figure 1A, compared with the control group, the weight of rats in the model group induced by TNBS decreased significantly ($p < 0.05$), and LZF significantly alleviated the trend of weight loss. The LZF-H group showed the strongest effect, which was significantly different from the model group. Figure 1B shows the DAI results of each group. The DAI was about 0 for the control group and continued at 8–10 for the model group, while LZF continued to reduce the DAI from the second day, with the LZF-H group decreasing most significantly compared to the model group ($p < 0.05$). Figures 1C,D show the appearance and length of the colon in each group; colon length results, showing that the model group had the shortest colon; and that the LZF-H group effectively inhibited the colon shortening caused by TNBS, with colons restored to normal length. In conclusion, the results of colitis-related indicators, including colon length, body weight, and DAI score, showed that LZF could significantly improve the UC caused by TNBS and that the therapeutic effect increased with dose.

3.2 Results of colonic tissue sections stained by H&E

H&E staining sections were used to observe the infiltration of inflammatory cells in colon tissue by comparing the morphology and size to reflect reduced inflammation in colon tissue (Zhang et al., 2021). The results of tissue sections (Figure 1E) showed that the structure of intestinal mucosa in the normal group was complete: the intestinal crypts were arranged orderly, and there was no edema in the submucosa. However, in the model group, the intestinal mucosa fell off, many inflammatory cells infiltrated, and the structure of intestinal recesses was seriously damaged. In the LZF-L group, the mucosa partially fell off and the recess structure remained intact, but there was inflammatory cell infiltration and obvious edema in the submucosa. In LZF-H group, the mucosal tissue fell off slightly, the recess structure was complete, and there was no edema in the submucosa. The microstructure of colon tissue showed that LZF could protect the normal physiological morphology of the colon and provide an intuitive basis for improving the effects of colitis.

3.3 Multivariate analysis of HPLC-QTOF-MS data

Mass spectrum information for serum samples in each group was obtained in positive and negative ion modes by HPLC-QTOF-MS. To find visual differences among the four groups, the multidimensional data after normalization, retention time correction, and peak picking were imported into SIMCA 14.0 software for multivariate statistical analysis. An overview of serum metabolic profiling was initially performed by a supervised PLS-DA analysis, which obtained more ideal

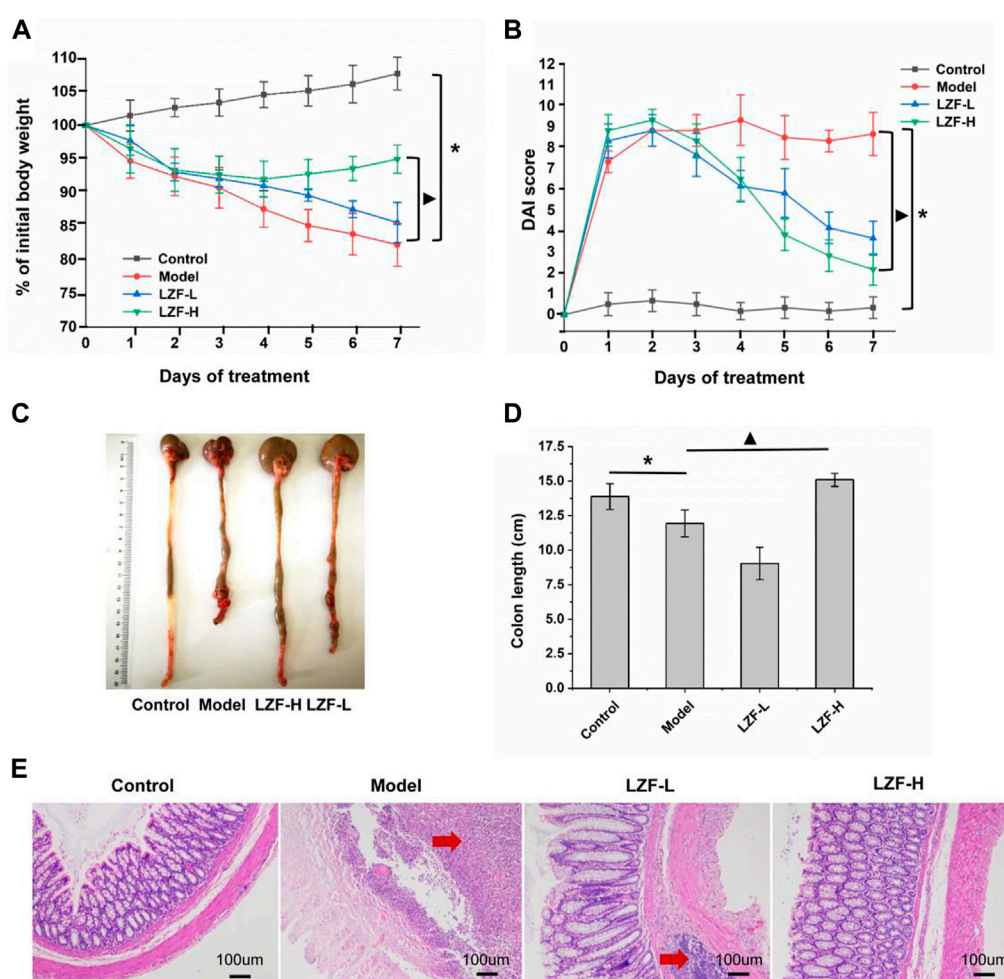


FIGURE 1

Therapeutic effect of LZF solution on ulcerative colitis caused by TNBS. (A) Body weight; (B) DAI score; (C) colon image; (D) colon length; and (E) histopathological section of colon.

intergroup separation and raised the identification of variables for the classification. To judge the reliability and accuracy of the model, PLS-DA score plots and 200 permutation test methods were provided for evaluation, as shown in Figures 2A–D. Among them, in the positive ion mode (Figure 2C), $R2X = 0.384$, $R2Y = 0.948$, and $Q2 = 0.602$; and in the negative ion mode (Figure 2D), $R2X = 0.447$, $R2Y = 0.911$, $Q2 = 0.601$, indicating that the model had not been over-fitted. The PLS-DA analysis indicated that serum samples for the control, model, LZF-L, and LZF-H groups showed clearly different classifications and separation in both positive and negative ion modes. The LZF-L and LZF-H groups were gradually closer to the normal group than to the model group. The TNBS-induced UC model could be considered successful. Therefore, these results show that the serum samples of each group had good separation, which is conducive to the further screening of differential metabolites.

To further differentiate metabolites between the two groups, OPLS-DA was used to better discriminate among the control and model groups, the model and LZF-L groups, and the model and LZF-H groups in both positive- and negative-ion modes. Based on the VIP value >1 , higher VIP values of metabolites indicated that these variables made significant contributions to the separation of each group. These results show that the OPLS-DA model exhibits favorable fitness and prediction.

3.4 Identification of structural elucidation of differential biomarkers

According to the VIP score of OPLS-DA for the samples in the aforementioned groups, combined with one-way ANOVA tests performed by SPSS software while the ions satisfying $VIP \geq$

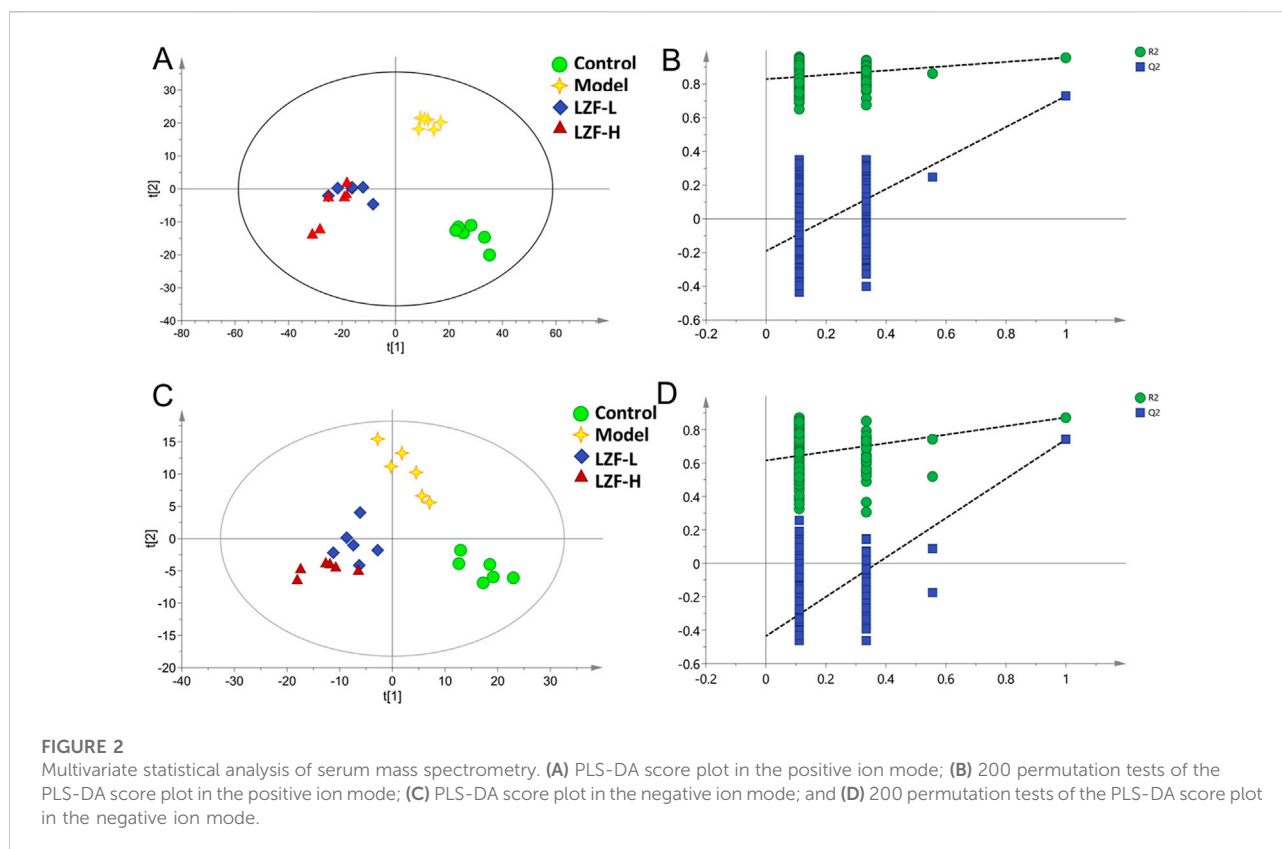
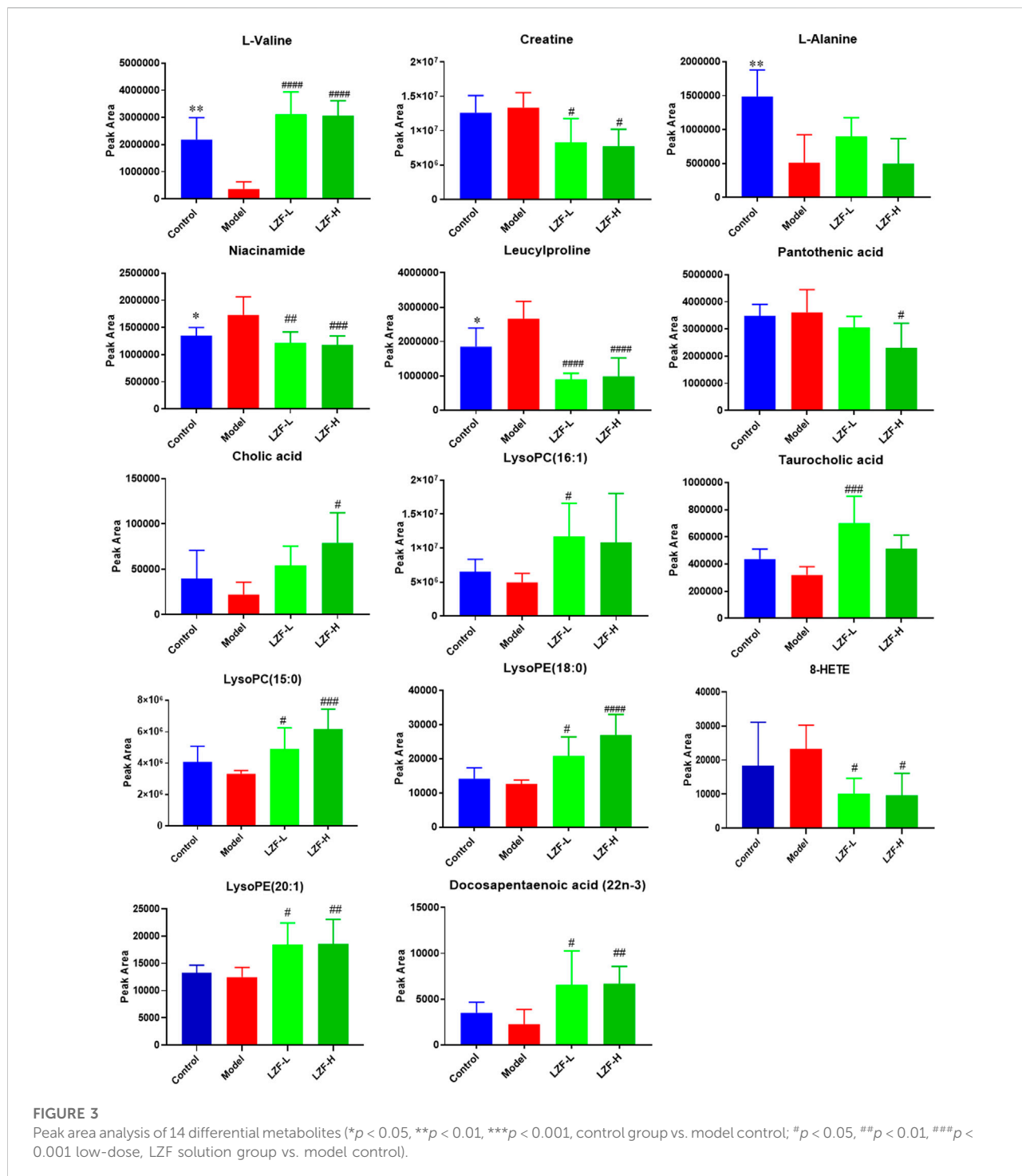


TABLE 1 Identified potential biomarkers of ulcerative colitis.

No.	Metabolite	Rt (min)	Determined mass (m/z)	Calculated mass (m/z)	Mass error (ppm)	Formula	Ion mode	VIP value	q-value
1	L-Valine	0.86	140.0681	140.0682	1	C ₅ H ₁₁ NO ₂	[M + Na] ⁺	4.05	<0.0001
2	Creatine	0.88	132.0772	132.0768	3	C ₄ H ₉ N ₃ O ₂	[M + H] ⁺	2.15	0.0059
3	L-Alanine	0.88	90.0557	90.0550	8	C ₃ H ₇ NO ₂	[M + H] ⁺	2.56	0.0018
4	Niacinamide	1.07	123.0554	123.0553	1	C ₆ H ₆ N ₂ O	[M + H] ⁺	1.75	0.0012
5	Leucylproline	1.50	229.1552	229.1547	2	C ₁₁ H ₂₀ N ₂ O ₃	[M + H] ⁺	3.35	0.0004
6	Pantothenic acid	2.09	220.1164	220.1179	7	C ₉ H ₁₇ NO ₅	[M + H] ⁺	2.49	0.0156
7	Cholic acid	8.13	407.2768	407.2803	9	C ₂₄ H ₄₀ O ₅	[M-H] ⁻	2.08	0.0237
8	LysoPC(16:1)	9.06	494.3224	494.3241	3	C ₂₄ H ₄₈ NO ₇ P	[M + H] ⁺	3.22	0.0471
9	Taurocholic acid	9.06	516.3033	516.2989	8	C ₂₆ H ₄₅ NO ₇ S	[M + H] ⁺	1.78	0.0078
10	LysoPC(15:0)	9.25	482.3217	482.3241	5	C ₂₃ H ₄₈ NO ₇ P	[M + H] ⁺	3.26	0.0011
11	LysoPE (18:0)	9.25	526.3118	526.3150	6	C ₂₃ H ₄₈ NO ₇ P	[M + FA-H] ⁻	1.41	<0.0001
12	8-HETE	9.95	319.2247	319.2279	10	C ₂₀ H ₃₂ O ₃	[M-H] ⁻	3.64	0.0262
13	LysoPE (20:1)	10.05	506.3218	506.3252	7	C ₂₅ H ₅₀ NO ₇ P	[M-H] ⁻	1.07	0.0038
14	Docosapentaenoic acid (22n-3)	13.62	329.2472	329.2486	4	C ₂₂ H ₃₄ O ₂	[M-H] ⁻	1.12	0.0311

1 and $p \leq 0.05$ were screened out, potential biomarkers were identified. A total of 35 metabolite ions with high VIP values were selected and isolated from serum samples for further

investigation. After a one-way ANOVA test based on accurate molecular mass measurement, fragmentation ions, peak mass spectrum data, and molecular formula, only 14 (including amino



acids, bile acids, fatty acids, peptides, and vitamins) were ultimately identified as potential biomarkers for control and model rats, as shown in Table 1. When the model group was adjusted up or down compared with the normal group, the LZF solution-treated group tended to call-back toward the normal group. Finally, the variation trend of these differential

metabolites was analyzed using one-way ANOVA adjusted by the FDR method, as shown by the statistical histogram drawn with the peak areas of the four groups in Figure 3.

Furthermore, combined with correlation analysis heat maps (in which blue indicates a negative correlation, red represents a positive correlation, and the color degree manifests the depth

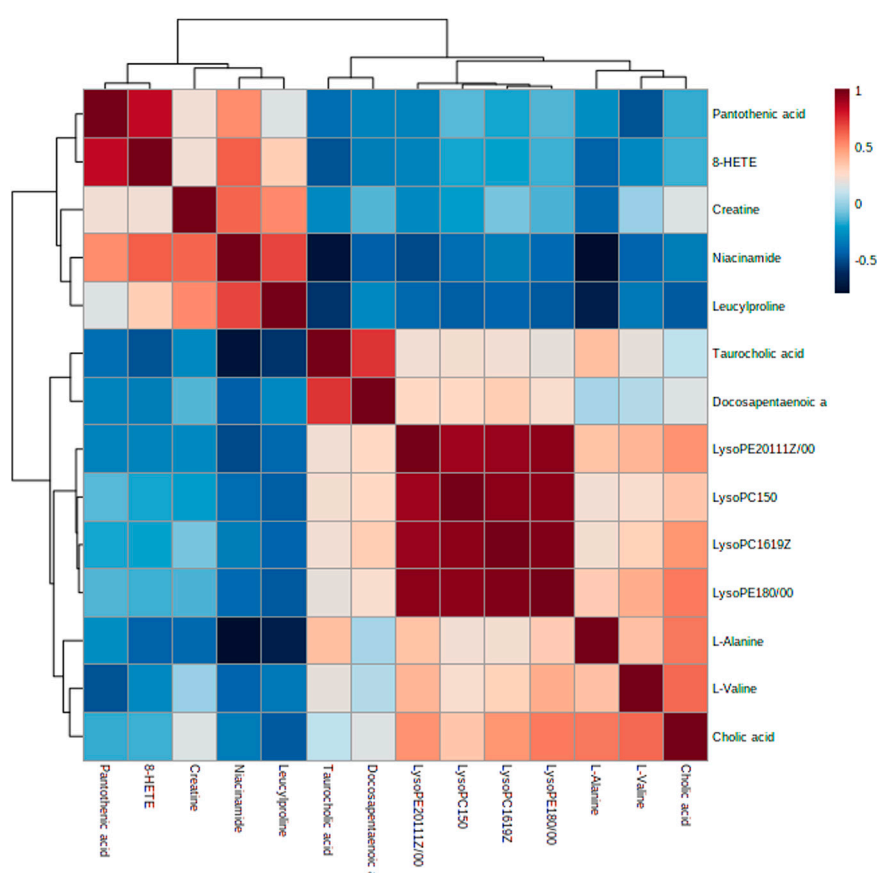


FIGURE 4
Correlation analysis of potential metabolite biomarkers in the LZF-L group compared to the model group.

correlation), the change trends of different metabolites biomarkers were determined (Figure 4) between the model and LZF-L groups. Five metabolites—creatine, niacinamide, leucylproline, pantothenic acid, and 8-HETE—accumulate with an elevated trend in the model group, while the other metabolites accumulate in a decreasing trend in LZF-L group. These results are consistent with the aforementioned results.

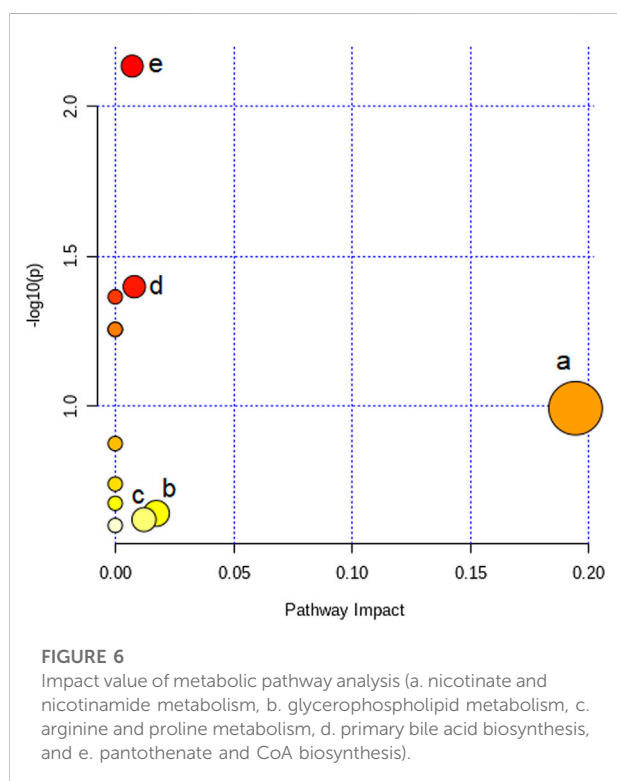
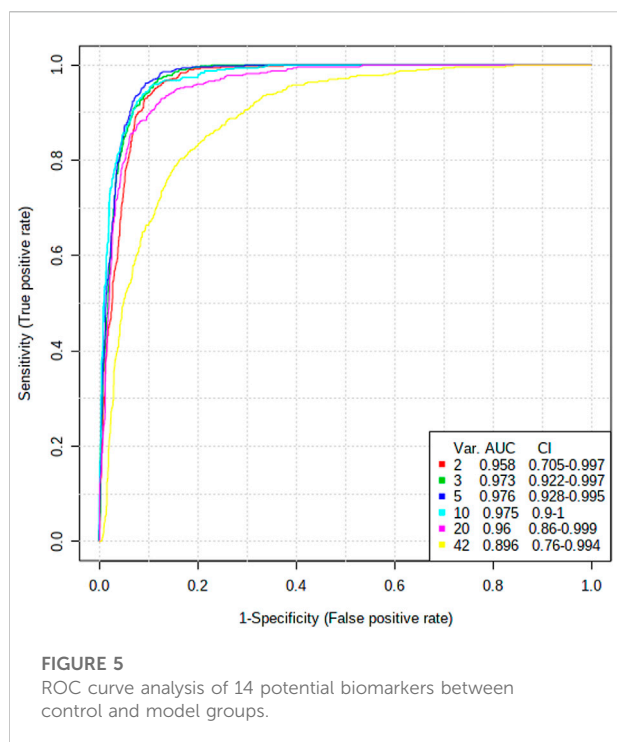
3.5 Diagnostic value analysis of diversified ROC curves

Characterizing the clinical diagnosis value of potential metabolomics biomarkers is a major task, and the utilization of receiver operating characteristic (ROC) curves to evaluate the diagnostic accuracy of biomarkers between the two groups has been successful in many studies (Wu et al., 2010). Area under the curve (AUC) is used to evaluate the clinical value of ROC curves, with biomarkers with AUC values greater than 0.8 being highly accurate and obviously differential (Broadhurst and Kell, 2006).

As shown in Figure 5, the AUC value is > 0.8, and the diagnostic sensitivity and specificity are high, indicating that these metabolites used as biomarkers for TNBS-induced UC disease diagnosis have high clinical diagnostic value. L-Alanine (AUC = 1.000), taurocholic acid (AUC = 0.917), niacinamide (AUC = 0.861), cholic acid (AUC = 0.861), and L-valine (AUC = 0.847) had AUC values higher than 0.8, suggesting that they can effectively contribute to TNBS-induced UC disease diagnosis.

3.6 Metabolic pathway analysis

To analyze the TNBS-induced UC metabolic pathway, the identified biomarkers related to UC were imported into MetaboAnalyst 4.0 software to determine which metabolic pathways were perturbed by the modeling. Twelve disturbed metabolic pathways were detected with large impact values (>0.00) and significant *p*-values (<0.05), including nicotinate and nicotinamide metabolism, glycerophospholipid metabolism, arginine and proline metabolism, primary bile acid biosynthesis, and pantothenate and CoA biosynthesis, as shown in Figure 6



and Table 2. The aforementioned pathways may be the potential mechanisms underlying changes in endogenous substance metabolism after treatment with LZF. In addition, various

metabolic pathways *in vivo* are interrelated, and LZF plays a synergistic role in multiple pathways. Therefore, the construction of a metabolic pathway interconnection network is conducive for describing the therapeutic mechanism of LZF solution in UC rats. As shown in Figure 7, the interaction of different metabolic pathways shows that UC is a disease involving multiple metabolic disorders that regulate amino acid metabolism, fat metabolism, and energy generation, while LZF could improve UC by regulating these metabolic pathways.

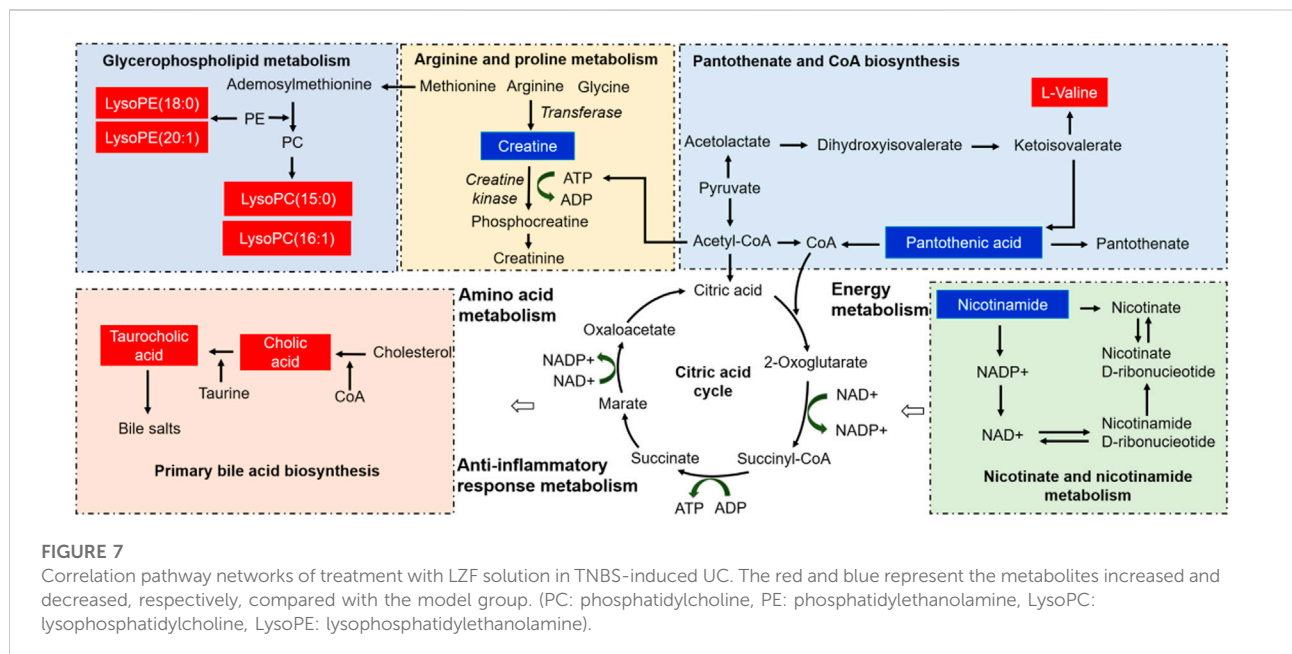
4 Discussion

Metabolomics has proved its capability and feasibility to explore the pharmacodynamics of botanical drugs and to reveal the intricate mechanisms of interactions between medicines and organisms. This study verified the therapeutic effect of the classic prescription of LZF on TNBS-induced UC rats. First, it confirmed that LZF has a good therapeutic effect on UC rats according to body weight, DAI, colon length, and pathological sections. Furthermore, HPLC-QTOF-MS was used to explore the mechanism of LZF on UC rats. A total of 14 potential biomarkers for the treatment of UC were identified, including amino acids, bile acids, lipid species (LysoPCs/LysoPEs), peptides, and vitamins. LZF plays a key role in regulating five significant metabolic pathways (pantothenate and CoA biosynthesis, nicotinate and nicotinamide metabolism, primary bile acid biosynthesis, glycerophospholipid metabolism, and arginine and proline metabolism) by normalizing energy production, amino acids, and inflammation in metabolic disorders. The following is a discussion of the biological significance of the aforementioned potential molecules and five aspects of dominant pathways to further reveal the mechanism of action of LZF on UC rats.

Energy metabolism is the most basic organic means of providing energy for all metabolic activities (Yu Z.W. et al., 2021). The treatment of UC rats with LZF solution mainly includes two energy metabolic pathways: pantothenic acid and CoA biosynthesis and niacin and nicotinamide metabolism. Both pantothenic acid and L-valine participate in the energy regulation pathways of pantothenate and CoA biosynthesis. Pantothenic acid, a B5 vitamin, participates in many metabolic reactions by synthesizing coenzyme A (CoA) to provide energy for the body (de Villiers et al., 2013). In addition, studies have shown that the energy production of colonic cells in patients with UC is reduced and that the conversion of bound pantothenic acid to CoA in the diseased mucosa is blocked, resulting in increased pantothenic acid serum levels associated with UC. Furthermore, L-valine is an essential amino acid that cooperates with pantothenic acid to regulate the pantothenate and CoA biosynthesis pathways. Previous studies have confirmed that compared with healthy people, the level of L-valine, a serum metabolite, is decreased in

TABLE 2 Summary of metabolic pathways of potential biomarkers.

Metabolic pathway	Total	Hits	Raw <i>p</i>	-log (<i>p</i>)	Impact	No. in Figure 6
Pantothenate and CoA biosynthesis	19	2	0.0073339	2.1347	0.00714	e
Primary bile acid biosynthesis	46	2	0.039973	1.3982	0.00805	d
Aminoacyl-tRNA biosynthesis	48	2	0.043228	1.3642	0	—
Valine, leucine, and isoleucine biosynthesis	8	1	0.055506	1.2557	0	—
Taurine and hypotaurine metabolism	8	1	0.055506	1.2557	0	—
Nicotinate and nicotinamide metabolism	15	1	0.10176	0.99242	0.1943	a
Selenocompound metabolism	20	1	0.13353	0.87443	0	—
Alanine, aspartate, and glutamate metabolism	28	1	0.18224	0.73936	0	—
Glycine, serine, and threonine metabolism	33	1	0.2114	0.67489	0	—
Glycerophospholipid metabolism	36	1	0.22844	0.64122	0.01736	b
Arginine and proline metabolism	38	1	0.23962	0.62048	0.01212	c
Valine, leucine, and isoleucine degradation	40	1	0.25064	0.60094	0	—



UC patients, which may be related to the downregulation of tryptophan hydroxylase in the rectal tissue of UC patients, thus leading to intestinal function disorder (Schicho et al., 2012). However, after the TNBS-induced UC rats were treated with LZF, the levels of pantothenic acid and L-valine were restored to normal, indicating that LZF profoundly regulates the damaged energy metabolism pathway and provides an important guarantee for other metabolic activities.

Nicotinamide is the key precursor of nicotinamide adenine dinucleotide (NAD⁺). Nicotinamide is mainly absorbed through the gastrointestinal mucosa and plays an important role in cellular energy metabolism through the

synthesis of NAD⁺. Recent studies have proved that nicotinamide also plays an important role in balancing intestinal dysfunction by regulating the inflammatory response, regulating the balance of the intestinal environment, and maintaining intestinal health (Shastri et al., 2020). Moreover, NAD⁺ generally regulates GPR109A and silent information regulator 2-related enzyme 1-mediated deacetylation to reduce the release of pro-inflammatory cytokines, including IL-1β, TNF-α, and NO (Chen et al., 2018). GPR109A and SIRT1 were widely expressed in colonic epithelial cells. In addition, SIRT1 is a positive regulator of NF-κB, which is considered to be an important

transcriptional factor in the production of pro-inflammatory cytokines (Ma et al., 2016). In this study, the colonic epithelial mucosa of TNBS-induced UC rats was damaged, and nicotinamide was more likely to enter the circulatory system and continuously accumulate in the blood vessels. The metabolism of nicotinic acid and nicotinamide is supersaturated, resulting in the inactivation of two important enzymes, NAMPT and NMNAT. However, after treatment with LZF, the content of nicotinamide in serum decreased, indicating that LZF mediates the expression of GPR109A and SIRT1 in colonic epithelial cells by activating the enzymes NAMPT and NMNAT, thus playing a regulatory role in the interrupted metabolism of nicotinic acid and nicotinamide. This could provide sufficient energy for lipid and amino acid metabolism, especially it could repair the intestinal mucosal barrier function and improve the inflammatory response.

During treatment in the UC rat model, two metabolic pathways were closely related to the inflammatory response: primary bile acid biosynthesis and glycerophospholipid metabolism. Cholic acid (CA) is a primary bile acid (BA) first catalyzed from cholesterol in liver, and it facilitates the digestion and absorption of dietary lipids and the fat-soluble vitamins A, D, E, and K into the intestine. Then the conjugation of CA to taurine by CoA synthetase forms taurocholic acid. Approximately 5% of the BAs then escape into the colon, where gut commensal bacteria convert them into various intestinal secondary bile acids that are pivotal hormones in regulating cholesterol metabolism, energy balance, intestinal motility, and bacterial growth, as well as inflammation *via* several nuclear receptors such as farnesoid X receptor, pregnane X receptor, vitamin D receptor, and 1 G protein-coupled receptor (Zhou et al., 2014; Song et al., 2020). In a previous study, primary bile acid biosynthesis was remarkably perturbed in some UC disorders, and treatment with oral administration of CA or CDCA improved lipid adsorption and inhibited the synthesis of toxic bile acid intermediates in the intestinal microenvironment (Heubi et al., 2018). In our study of UC disease, treatment with LZF solution led to upregulated levels of cholic acid and taurocholic acid compared to the control group. This finding clarifies that UC disease with gut mucosal barrier and inflammation dysfunction can cause abnormal primary bile acid metabolism, which leads to bile acid enterohepatic circulation being blocked in the colon; the amount of bile acid returning to the liver was reduced, and the level of bile acid in serum decreased. These results indicate that LZF solution regulates the disrupted primary bile acid biosynthesis and regulates the BA-induced TGR5 signaling pathway with intestinal macrophages.

Glycerophospholipid metabolism participates in the regulation of inflammatory response through the synthesis of its derivative lysosomes. Glycerophospholipids are the

structural components of cell membranes and contain many derivatives of glycerophosphoric acid, including lysophosphatidylcholines (LysoPCs) and lysophosphatidylethanolamines (LysoPEs). In general, LysoPCs have strong surface activity which can rupture red blood cells, changing their permeability and causing hemolysis or cell necrosis, and release histamine, serotonin, and epinephrine, stimulating a series of complex pathological reactions at the intestinal barrier as well as pro-inflammatory effects. However, unsaturated LysoPCs, such as LysoPC (15:0) and LysoPC (16:1), are potentially protective factors in inflammation, while saturated LysoPCs, such as LysoPC (18:0) and LysoPC (18:1), have been shown to promote proinflammatory cytokine release and exacerbate the inflammatory process (Jia et al., 2018; Guan et al., 2020). Moreover, previous studies have confirmed the presence of disturbed glycerophospholipids in patients and animals with UC (Wang et al., 2016). For example, dysregulation of the intestinal flora in IBD-model animals may lead to downregulation of glycerophospholipid synthesis, and the number of LysoPCs and LysoPEs in their serum has also been found to be reduced (Lu et al., 2012). In our study, LysoPC (15:0), LysoPC (16:1), and LysoPE (18:0) were upregulated upon LZF treatment in TNBS-induced UC, compared to the model group. These results are consistent with the favorable effects of unsaturated LysoPCs on the intestinal barrier and anti-inflammatory properties and indicate that some LysoPCs play roles in preventing mucosal inflammation to inhibit pivotal pro-inflammatory factors including IL-8, NO, and TNF- α in UC disease.

A previous study has shown the intestinal epithelium to have increased hypoxic stress and acutely increased energy requirements in the inflammation response of UC rats after induction with DSS, a metabolic stressor of epithelial cells (Turer et al., 2017). Creatine, an amino acid, is synthesized from three amino acids (glycine, arginine, and methionine), then exported from the liver to blood vessels (Brosnan and Brosnan, 2016). Creatine is interconverted to phosphocreatine and ADP in tissue cells with a rapid, high demand for creatine kinase and ATP. Therefore, the requirement for rapid ATP replenishment for amino acid metabolism *in vivo* within the colonic mucosal barrier plays an essential role in regulating intestinal homeostasis and protecting against UC. In our study, the creatine level in the model group was lower than that in the control group due to insufficient ATP energy supply in TNBS-induced UC rats. We inferred that tissue uptake of creatine would be blocked, resulting in increased content and accumulation, and would further disrupt arginine and proline metabolism. With the treatment of LZF solution, which ameliorates altered metabolites and pathways to repair the colonic barrier function, creatine is downregulated by normal energy metabolism functions with high CoA levels and increased ATP synthesis in cells. These results indicate

that amino acid metabolisms containing creatine play important biological roles in UC disease, directly or indirectly linking energy metabolism with intestinal homeostasis by inhibiting inflammation and reducing oxidative stress.

In summary, the experimental results indicate that LZJ solution plays a crucial role in metabolites in the treatment of UC and the regulation of main pathways of energy metabolism, anti-inflammatory response metabolism, and amino acid metabolism. Although this study has successfully identified specific UC biomarkers using serum metabolomics combined with HPLC-QTOF-MS technology, it has certain limitations. First, all active differential metabolites using metabolomics combined with genomics and proteomics in serum, urine, feces, colon tissue, and liver tissue of rats should be screened and analyzed by GC-MS, NMR, or HPLC-QTOF-MS to further clarify the full biological effects and bioactive integrated mechanisms of LZJ solution in the treatment of UC. Second, Western blot and PCR studies should be used to elucidate essential protein pathways and related factors. Third, we should demonstrate the interplay of the gut microbiota and colon mucosa in anti-inflammatory processes. Such in-depth studies will better provide approaches to understanding the key metabolites and comprehensive metabolic pathways of the mechanism of treatment of UC.

5 Conclusion

Based on LZJ's anti-UC effect, this study used metabolomics technology to study its possible metabolic pathway, which provided a basis for revealing the mechanism of LZJ in the treatment of UC. LZJ showed excellent anti-UC effects and significantly inhibited the disease characteristics of weight loss, increased DAI, colon shortening, and inflammatory infiltration of intestinal tissue in rats by TNBS, and the effect was dose-dependent. Metabolomics study found 14 potential biomarkers, involving 12 metabolic pathways, among which the most significant ones included nicotinate and nicotinamide metabolism, glycerophospholipid metabolism, arginine and proline metabolism, primary bile acid biosynthesis, and pantothenate and CoA biosynthesis. Therefore, LZJ improves UC by regulating amino acid metabolism, fat metabolism, and energy production.

References

Alatab, S., Sepanlou, S. G., Ikuta, K., Vahedi, H., Bisignano, C., Safiri, S., et al. (2020). The global, regional, and national burden of inflammatory bowel disease in 195 countries and territories, 1990–2017: a systematic analysis for the global burden of disease study 2017. *Lancet. Gastroenterol. Hepatol.* 5, 17–30. doi:10.1016/S2468-1253(19)30333-4

Data availability statement

The original contributions presented in the study are included in the article/Supplementary Material; further inquiries can be directed to the corresponding authors.

Ethics statement

The animal study was reviewed and approved by the Chengdu University of Traditional Chinese Medicine.

Author contributions

JB and TX performed the animal studies. XW performed the metabolomics study. YC performed the H&E analysis and the pharmacological experiments. RL performed the computational analysis. CF conceived the design of the study. XY supervised the study. All authors participated in the interpretation of experimental results and in drafting the manuscript.

Funding

This work was supported by the Innovation Team and Talents Cultivation Program of the National Administration of Traditional Chinese Medicine (No: ZYYCXTD-D-202209).

Conflict of interest

The authors declare that the research was conducted in the absence of any commercial or financial relationships that could be construed as a potential conflict of interest.

Publisher's note

All claims expressed in this article are solely those of the authors and do not necessarily represent those of their affiliated organizations, or those of the publisher, the editors, and the reviewers. Any product that may be evaluated in this article, or claim that may be made by its manufacturer, is not guaranteed or endorsed by the publisher.

Broadhurst, D. I., and Kell, D. B. (2006). Statistical strategies for avoiding false discoveries in metabolomics and related experiments. *Metabolomics* 2, 171–196. doi:10.1007/s11306-006-0037-z

Brosnan, M. E., and Brosnan, J. T. (2016). The role of dietary creatine. *Amino Acids* 48, 1785–1791. doi:10.1007/s00726-016-2188-1

- Chen, G., Huang, B., Fu, S., Li, B., Ran, X., He, D., et al. (2018). G protein-coupled receptor 109A and host microbiota modulate intestinal epithelial integrity during sepsis. *Front. Immunol.* 9, 2079. doi:10.3389/fimmu.2018.02079
- De Villiers, M., Macuamule, C., Spry, C., Hyun, Y. M., Strauss, E., and Saliba, K. J. (2013). Structural modification of pantothenamides counteracts degradation by pantothenase and improves antiparasitodal activity. *ACS Med. Chem. Lett.* 4, 784–789. doi:10.1021/ml400180d
- Guan, S., Jia, B., Chao, K., Zhu, X., Tang, J., Li, M., et al. (2020). UPLC-QTOF-MS-Based plasma lipidomic profiling reveals biomarkers for inflammatory bowel disease diagnosis. *J. Proteome Res.* 19, 600–609. doi:10.1021/acs.jproteome.9b00440
- He, Y., Chen, Z., Nie, X., Wang, D., Zhang, Q., Peng, T., et al. (2022). Recent advances in polysaccharides from edible and medicinal *Polygonati rhizoma*: From bench to market. *Int. J. Biol. Macromol.* 195, 102–116. doi:10.1016/j.ijbiomac.2021.12.010
- Heubi, J. E., Setchell, K. D. R., and Bove, K. E. (2018). Inborn errors of bile acid metabolism. *Clin. Liver Dis.* 22, 671–687. doi:10.1016/j.cld.2018.06.006
- Hoivik, M. L., Moum, B., Solberg, I. C., Henriksen, M., Cvancarova, M., Bernklev, T., et al. (2013). Work disability in inflammatory bowel disease patients 10 years after disease onset: results from the IBSEN study. *Gut* 62, 368–375. doi:10.1136/gutjnl-2012-302311
- Hong, Z.-C., Cai, Q., Wu, H.-Z., Yang, Y.-F., Fan, H., and Duan, X.-Y. (2021). Compound Sophorae decoction: treating ulcerative colitis by affecting multiple metabolic pathways. *Chin. J. Nat. Med.* 19, 267–283. doi:10.1016/S1875-5364(21)60029-8
- Jia, W., Xie, G., and Jia, W. (2018). Bile acid-microbiota crosstalk in gastrointestinal inflammation and carcinogenesis. *Nat. Rev. Gastroenterol. Hepatol.* 15, 111–128. doi:10.1038/nrgastro.2017.119
- Kobayashi, T., Siegmund, B., Le Berre, C., Wei, S. C., Ferrante, M., Shen, B., et al. (2020). Ulcerative colitis. *Nat. Rev. Dis. Prim.* 6, 74. doi:10.1038/s41572-020-0205-x
- Li, H., Fan, C., Lu, H., Feng, C., He, P., Yang, X., et al. (2020). Protective role of berberine on ulcerative colitis through modulating enteric glial cells-intestinal epithelial cells-immune cells interactions. *Acta Pharm. Sin. B* 10, 447–461. doi:10.1016/j.apsb.2019.08.006
- Li, Y. H., Xiao, H. T., Hu, D. D., Fatima, S., Lin, C. Y., Mu, H. X., et al. (2016). Berberine ameliorates chronic relapsing dextran sulfate sodium-induced colitis in C57BL/6 mice by suppressing Th17 responses. *Pharmacol. Res.* 110, 227–239. doi:10.1016/j.phrs.2016.02.010
- Liao, Z., Xie, Y., Zhou, B., Zou, B., Xiao, D., Liu, W., et al. (2020). Berberine ameliorates colonic damage accompanied with the modulation of dysfunctional bacteria and functions in ulcerative colitis rats. *Appl. Microbiol. Biotechnol.* 104, 1737–1749. doi:10.1007/s00253-019-10307-1
- Lu, K., Knutson, C. G., Wishnok, J. S., Fox, J. G., and Tannenbaum, S. R. (2012). Serum metabolomics in a *Helicobacter hepaticus* mouse model of inflammatory bowel disease reveal important changes in the microbiome, serum peptides, and intermediary metabolism. *J. Proteome Res.* 11, 4916–4926. doi:10.1021/pr300429x
- Lu, Y., Chen, J., He, X., Xu, S., Chen, Y. E., Gao, J., et al. (2021). Combined administration of vitamin D3 and geniposide is less effective than single use of vitamin D3 or geniposide in the treatment of ulcerative colitis. *Front. Pharmacol.* 12, 714065. doi:10.3389/fphar.2021.714065
- Ma, Y., Bao, Y., Wang, S., Li, T., Chang, X., Yang, G., et al. (2016). Anti-inflammation effects and potential mechanism of saikosaponins by regulating nicotinate and nicotinamide metabolism and arachidonic acid metabolism. *Inflammation* 39, 1453–1461. doi:10.1007/s10753-016-0377-4
- Schicho, R., Shaykhtudinov, R., Ngo, J., Nazyrova, A., Schneider, C., Panaccione, R., et al. (2012). Quantitative metabolomic profiling of serum, plasma, and urine by ¹H NMR spectroscopy discriminates between patients with inflammatory bowel disease and healthy individuals. *J. Proteome Res.* 11, 3344–3357. doi:10.1021/pr300139q
- Shastri, S., Shinde, T., Sohal, S. S., Gueven, N., and Eri, R. (2020). Idebenone protects against acute murine colitis via antioxidant and anti-inflammatory mechanisms. *Int. J. Mol. Sci.* 21, E484. doi:10.3390/ijms21020484
- Song, X., Sun, X., Oh, S. F., Wu, M., Zhang, Y., Zheng, W., et al. (2020). Microbial bile acid metabolites modulate gut RORγ+ regulatory T cell homeostasis. *Nature* 577, 410–415. doi:10.1038/s41586-019-1865-0
- Sun, L. M., Zhu, B. J., Cao, H. T., Zhang, X. Y., Zhang, Q. C., Xin, G. Z., et al. (2018). Explore the effects of Huang-Lian-Jie-Du-Tang on Alzheimer's disease by UPLC-QTOF/MS-based plasma metabolomics study. *J. Pharm. Biomed. Anal.* 151, 75–83. doi:10.1016/j.jpba.2017.12.053
- Turer, E., Mcalpine, W., Wang, K. W., Lu, T., Li, X., Tang, M., et al. (2017). Creatine maintains intestinal homeostasis and protects against colitis. *Proc. Natl. Acad. Sci. U. S. A.* 114, E1273–E1281. doi:10.1073/pnas.1621400114
- Ungaro, R., Mehandru, S., Allen, P. B., Peyrin-Biroulet, L., and Colombel, J.-F. (2017). Ulcerative colitis. *Lancet* 389, 1756–1770. doi:10.1016/S0140-6736(16)32126-2
- Wang, M., Chen, L., Liu, D., Chen, H., Tang, D. D., and Zhao, Y. Y. (2017). Metabolomics highlights pharmacological bioactivity and biochemical mechanism of traditional Chinese medicine. *Chem. Biol. Interact.* 273, 133–141. doi:10.1016/j.cbi.2017.06.011
- Wang, R., Gu, X., Dai, W., Ye, J., Lu, F., Chai, Y., et al. (2016). A lipidomics investigation into the intervention of celastrol in experimental colitis. *Mol. Biosyst.* 12, 1436–1444. doi:10.1039/c5mb00864f
- Wang, W., Xu, C., Li, X., Wang, Z., Yang, J., Shen, Y., et al. (2021). Exploration of the potential mechanism of Banxia Xiexin Decoction for the effects on TNBS-induced ulcerative colitis rats with the assistance of network pharmacology analysis. *J. Ethnopharmacol.* 277, 114197. doi:10.1016/j.jep.2021.114197
- Wang, X., Zhang, C., Zheng, M., Gao, F., Zhang, J., and Liu, F. (2019). Metabolomics analysis of L-arginine induced gastrointestinal motility disorder in rats using UPLC-MS after magnolol treatment. *Front. Pharmacol.* 10, 183. doi:10.3389/fphar.2019.00183
- Wu, H., Xue, R., Tang, Z., Deng, C., Liu, T., Zeng, H., et al. (2010). Metabolomic investigation of gastric cancer tissue using gas chromatography/mass spectrometry. *Anal. Bioanal. Chem.* 396, 1385–1395. doi:10.1007/s00216-009-3317-4
- Xiang, Z., Xie, H., Tong, Q., Pan, J., Wan, L., Fang, J., et al. (2021). Revealing hypoglycemic and hypolipidemic mechanism of Xiaokeyinshui extract combination on streptozotocin-induced diabetic mice in high sucrose/high fat diet by metabolomics and lipidomics. *Biomed. Pharmacother.* 135, 111219. doi:10.1016/j.biopha.2021.111219
- Yang, H., Yue, Y., Li, Y., Su, L., and Yan, S. (2020). Geniposide attenuates dextran sulfate sodium-induced colitis in mice via Nrf-2/HO-1/NF-κB pathway. *Ann. Palliat. Med.* 9, 2826–2836. doi:10.21037/apm-20-279
- Yang, Y., Zhu, X., Qin, Y., Chen, G., Zhou, J., Li, L., et al. (2017). The anti-inflammatory effect of guchangzhixie-pill by reducing colonic EC cell hyperplasia and serotonin availability in an ulcerative colitis rat model. *Evid. Based. Complement. Altern. Med.* 2017, 8547257. doi:10.1155/2017/8547257
- Yu, T., Li, Z., Xu, L., Yang, M., and Zhou, X. (2021). Anti-inflammation effect of Qingchang suppository in ulcerative colitis through JAK2/STAT3 signaling pathway *in vitro* and *in vivo*. *J. Ethnopharmacol.* 266, 113442. doi:10.1016/j.jep.2020.113442
- Yu, Z. W., Xie, Y., Huang, Z. C., Yang, K., Wang, Z. G., and Hu, H. L. (2021). Study of the therapeutic effect of raw and processed *Vladimiriae Radix* on ulcerative colitis based on intestinal flora, metabolomics and tissue distribution analysis. *Phytomedicine*. 85, 153538. doi:10.1016/j.phymed.2021.153538
- Yuan, Z., Yang, L., Zhang, X., Ji, P., Hua, Y., and Wei, Y. (2020). Mechanism of Huang-lian-jie-du decoction and its effective fraction in alleviating acute ulcerative colitis in mice: Regulating arachidonic acid metabolism and glycerophospholipid metabolism. *J. Ethnopharmacol.* 259, 112872. doi:10.1016/j.jep.2020.112872
- Zhang, C., Jiang, M., and Lu, A. (2013). Considerations of traditional Chinese medicine as adjunct therapy in the management of ulcerative colitis. *Clin. Rev. Allergy Immunol.* 44, 274–283. doi:10.1007/s12016-012-8328-9
- Zhang, C., Li, J., Xiao, M., Wang, D., Qu, Y., Zou, L., et al. (2022a). Oral colon-targeted mucoadhesive micelles with enzyme-responsive controlled release of curcumin for ulcerative colitis therapy. *Chin. Chem. Lett.* 33, 4924–4929. doi:10.1016/j.ccllet.2022.03.110
- Zhang, C., Wang, X., Xiao, M., Ma, J., Qu, Y., Zou, L., et al. (2022b). Nano-in-micro alginate/chitosan hydrogel via electrospray technology for orally curcumin delivery to effectively alleviate ulcerative colitis. *Mater. Des.* 221, 110894. doi:10.1016/j.matdes.2022.110894
- Zhang, S., Kang, L., Hu, S., Hu, J., Fu, Y., Hu, Y., et al. (2021). Carboxymethyl chitosan microspheres loaded hyaluronic acid/gelatin hydrogels for controlled drug delivery and the treatment of inflammatory bowel disease. *Int. J. Biol. Macromol.* 167, 1598–1612. doi:10.1016/j.ijbiomac.2020.11.117
- Zhang, Z., Li, Y., Shen, P., Li, S., Lu, X., Liu, J., et al. (2017). Administration of geniposide ameliorates dextran sulfate sodium-induced colitis in mice via inhibition of inflammation and mucosal damage. *Int. Immunopharmacol.* 49, 168–177. doi:10.1016/j.intimp.2017.05.033
- Zhou, X., Cao, L., Jiang, C., Xie, Y., Cheng, X., Krausz, K. W., et al. (2014). PPARα-UGT axis activation represses intestinal FXR-PGF15 feedback signalling and exacerbates experimental colitis. *Nat. Commun.* 5, 4573. doi:10.1038/ncomms5573

连栝矾溶液改善结直肠炎的作用机制研究

肛肠疾病除了痔瘕类疾病以外，还包含慢性肠炎，其中结直肠炎（保留灌肠）为慢性肠炎的代表性疾病，是一种慢性非特异性炎症性肠病，临床表现为肠道炎症、组织损伤、腹痛、频繁或持续腹泻、直肠出血等，反复发作难治愈，严重影响患者生活质量^[69-70]，因此本章拟围绕结直肠炎（保留灌肠）开展药效机制研究，探索连栝矾溶液对肛肠特色疾病的药效作用和机制。

代谢组学是继基因组学、蛋白质组学、转录组学后新近发展起来的一门学科，通过高通量检测等技术手段从代谢物层面探究细胞内的生命活动，对生物体内的内源性代谢物进行定性定量分析，从系统、整体的角度对生物体的内源变化进行解释^[71]。整体观念是中医的基本特点之一，代谢组学可以全面地、整体地、系统地、动态地研究外源性中药对于机体代谢状态的影响，研究方法与中医整体观点不谋而合，在阐明中药复方多成分、多靶点、多通路的治疗机制中展现出良好的应用前景^[72]。

连栝矾溶液是由黄连、栝子和白矾水煎液经发酵制备而成的中药院内制剂，在我国临床上用于治疗肛瘘、肛周脓肿、慢性肠炎等肛肠疾病已有数百年历史。结直肠炎为慢性肠炎的代表性疾病，由于中药的复杂性，连栝矾溶液治疗结直肠炎（保留灌肠）的潜在机制尚不清楚，因此本部分在第一节研究结果的基础上，拟采用最佳体外抗炎组分即发酵后的连栝矾溶液，建立 2,4,6-三硝基苯磺酸（2,4,6-trinitrobenzenesulfonic acid, TNBS）诱导的溃疡性结肠炎（UC）大鼠模型，进一步探索其改善结直肠炎（保留灌肠）的药效和作用机制；同时拟采用高效液相色谱 - 四极杆 - 飞行时间串联质谱 (Ultra High Performance Liquid Chromatography-Quadrupole Time of Flight Mass Spectrometry, HPLC-Q-TOF-MS/MS)

分析介导的代谢组学方法，结合质谱信息和公共数据库检索，筛选血清中差异代谢物及所属代谢通路，探索连翘酚溶液治疗结直肠炎（保留灌肠）的特异性生物标志物及潜在代谢机制。

1.仪器与材料

1.1 仪器

名称	厂家	型号
高效液相色谱仪	Agilent	Agilent1200
Q-TOF-MS	Agilent	Agilent 6530
MX-F 型涡旋混合器	武汉赛维尔生物科技有限公司	MX-F
纯水机	四川优普超纯科技有限公司	UPK-I-10T
数控超声波清洗器	上海之信仪器有限公司	DL-720D
扫描浏览软件	3DHISTECH (Hungary)	CaseViewer
全景切片扫描仪	3DHISTECH (Hungary)	PANNORAMIC150
快速组织脱水机	Thermo scientific/赛默飞世尔	STP420 ES
包埋机	武汉俊杰电子有限公司	JB-P5
冻台	武汉俊杰电子有限公司	JB-L5
修蜡仪	武汉俊杰电子有限公司	JXL-818
切片机	Thermo scientific/赛默飞世尔	HM325
组织摊烤片机	武汉俊杰电子有限公司	JK-6
全自动染色机	Thermo scientific/赛默飞世尔	Varistain™ Gemini ES
封片机	Thermo scientific/赛默飞世尔	Autostainer 360
电热鼓风干燥箱（烤箱）	上海一恒科学仪器有限公司	DHG-9240A
载玻片	南通美韦德实验器材有限公司	220518001
盖玻片	南通美韦德实验器材有限公司	220518001
包埋盒打号机	Thermo scientific/赛默飞世尔	PrintMate AS

1.2 药品与试剂

试剂	厂家
5 %TNBS	美国 Sigma 奥尔德里奇公司
连翘砒溶液	成都肛肠专科医院
多聚甲醛	美国 Sigma 奥尔德里奇公司
氯化钠注射液	四川科伦药业股份有限公司
二甲苯	成都市科隆化学品有限公司
无水乙醇	成都市科隆化学品有限公司
HE 染液套装	Leagene
盐酸	四川西陇科学有限公司
氨水	成都市科隆化学品有限公司
中性树脂	国药集团化学试剂有限公司

1.3 实验动物

雄性 (Sprague – Dawley, SD) 大鼠 (180 ~ 200 g), 购自成都达硕生物科技有限公司。大鼠饲养于 (温度 20 ~ 23 °C, 湿度 50 ± 10 %, 通风换气 8 次/h) 标准条件下, 自由进食和饮水。所有动物实验均按照成都中医药大学实验动物福利伦理委员会批准的实验方案进行。

2. 方法

2.1 动物造模及分组、给药

将 24 只 SD 大鼠随机分为 4 组, 每组 6 只, 分别命名为对照组、模型组、连翘砒溶液高剂量组 (LZF-H) 和连翘砒溶液低剂量组 (LZF-L)。适应性喂养后, 对

照组大鼠给予 0.9%生理盐水溶液，其余各组大鼠于距肛门 8 cm 处插入 TNBS 溶液 (30 mg/kg，溶于 50%乙醇)诱导溃疡性结肠炎^[73]。连梳矾溶液高剂量组和连梳矾溶液低剂量组分别按连梳矾溶液 2 mL 和 1 mL 结肠给药，对照组和模型组大鼠结肠给予 0.9%生理盐水溶液，每日 1 次，连续 7 d。

2.2 大鼠疾病指数评分

整个实验过程中，每天观察并记录大鼠体重变化情况，同时记录大鼠粪便性状，便血情况，评分标准分为五级，具体疾病指数评分表 (Disease Activity Index, DAI) 见表 3-1。

表 3-1 DAI 评分表
Table 3-1. The scores for DAI (Disease Activity Index)

评分	体重减少 (%)	大便性状	便血
0	<5	正常	无
1	5-10	软便	隐血
2	10-15	稀便	隐血
3	15-20	腹泻	肉眼可见血
4	>20	严重腹泻	大便出血

2.3 样品采集与制备

末次给药后禁食 24 h，戊巴比妥钠麻醉，腹主动脉取血。血液在 4 °C 下凝固 2 h 后，3500 rpm 离心 10 min。将上清液样品转移至微量离心管 (eppendorf, EP) 中，立即保存于 -80 °C 直至分析。解剖大鼠，取出距肛门 8 cm 处结肠组织，沿肠系膜缘剪开肠腔，用生理盐水冲洗肠内容物，测量结肠长度并拍照。取一部分结肠肠段置于多聚甲醛浸泡，用于苏木精-伊红染色法 (hematoxylin-eosin staining, HE) 染色。

2.4 HE 染色法观测结肠组织病理情况

切取各组大鼠结肠组织浸于 4%多聚甲醛中固定 24 h 后更换固定液，48 h 后进

行脱水→透明→浸蜡→石蜡包埋，冰冻蜡块后用切片机切成 4 μm 厚度，再烤片烘干备用。将组织切片进行逐级脱蜡：依次将切片放入二甲苯 I 20 min-二甲苯 II 20 min-无水乙醇 I 5 min-无水乙醇 II 5 min-75%乙醇 5 min，自来水洗；然后采用苏木精染色 3-5 min，盐酸水溶液分化，氨水水溶液返蓝，水洗；再将切片依次入 85%、95%的梯度酒精脱水，入伊红染液中染色 5 min；最后将切片依次放入无水乙醇 I 5 min -无水乙醇 II 5 min-无水乙醇 III 5 min -二甲苯 I 5 min- 二甲苯 II 5 min 透明，用中性树胶封片。最后在光学显微镜下观察组织结构并且随机选取视野进行拍照记录，观察大鼠结肠的形态学变化：上皮细胞形态、炎症细胞浸润情况、隐窝结构变化。

2.5 血清样本代谢组学分析

2.5.1 血清样品的制备

4 °C 下解冻血清样本，取 100 μL 样本至离心管中，加入 400 μL 甲醇 (-20 °C)，将混合物涡旋 10 min，使之充分混匀，然后于 4 °C 下，12000 rpm 离心 10 min，取全部上清液。将上清液样品真空浓缩至干燥，然后复溶，高低剂量组给药体积不一致 0.22 μm 微孔滤膜滤过，得到用于 HPLC-Q-TOF-MS 分析血清样品。从每组中每个样品随机抽取 20 μL 混匀，作为质量控制样品用于方法验证，以消除实验的系统误差。

2.5.2 HPLC-Q-TOF-MS 条件

所有分析均在 Agilent 1200 系列高效液相色谱仪 (Agilent 公司，德国) 上进行。色谱分离采用 ACE Excel C₁₈ 色谱柱 (100 mm × 2.1 mm, 3.0 mm)，柱温 40 °C。流动相由 (A) 0.1 % (v/v) 甲酸水溶液和 (B) 含 0.1 %甲酸的乙腈组成，流速 0.4 mL·min⁻¹。血清样品梯度洗脱程序表见表 3-2。样品进样量设定为 3 μL。

表 3-2 血清样品梯度洗脱程序表

Table 3-2 Gradient elution procedure for serum samples

时间 (min)	流动相 A (%)	流动相 B (%)
0~2	95	5

2~7	95~35	5~65
7~20	35~5	65~95
20~22	5	95
22~23	5~95	95~5
22~28	95	5

采用结合电喷雾离子源(ESI)进行质谱(MS)分析。系统运行采用 MassHunter 工作站软件(美国 Agilent Technologies 公司)。质谱条件:毛细管电压,正离子模式 4.0 kV,负离子模式 3.5 kV;雾化器压力 35 psig;气体温度 320 °C;气体流量 12 L/min;碰撞能量为 35 eV;干燥气温度为 300 °C,干燥气流量为 6 L/min。全扫描模式设定质量范围为 50 ~ 1100 Da。

2.5.3 数据处理及多因素分析

通过 HPLC-Q-TOF-MS 收集基峰色谱 (Base peak chromatography, BPC) 数据,将得到的原始数据通过 MSConvert 软件 (3.0 版本,美国 ProteoWizard 公司)转换成 mzXML 格式。然后将文档导入 XCMS 网站软件 (<https://xcmsonline.edu>) 进行噪声去除、基线校正、峰对齐等操作,自动生成由保留时间、峰强度和质荷比 (m/z) 组成的多维数据矩阵的 tsv 文档。通过"80 %校正法"重新获得"tsv"文件中的最终峰面积。

将预处理后的数据文件导入 SIMCA (ver.14.0) 软件包 (Umetrics, Umea, 瑞典)进行多元统计分析,包括无监督主成分分析 (Principal Component Analysis, PCA)、偏最小二乘判别分析 (Partial Least Squares-Discriminant Analysis, PLS-DA) 和有监督的正交-偏最小二乘判别分析 (Orthogonal Partial Least Squares Discriminant Analysis, OPLS-DA) 进行统计分析,用于根据内源性代谢物探讨组间差异,并选择 VIP 值 ($VIP > 1.5$) 来显示变异的贡献。这些差异潜在代谢物被认为是潜在的化学标志物。采用 Graph Pad Prism 软件 (version 9.0, GraphPad, USA) 对数据进行分析,采用单因素方差分析检验不同组间的显著性差异 ($p < 0.05$)。

2.5.4 生物标志物鉴定及通路分析

通过筛选潜在的代谢物，根据保留时间、MS 和 MS/MS 精确质量数以及元素组成数据进行生物标志物的鉴定，通过比较各种数据库如人类代谢组数据库 (<http://www.hmdb.ca>)，KEGG (<http://www.genome.jp/kegg/>) 的结果，进一步通过 MetaboAnalyst Database (<http://www.metaboanalyst.ca/>) 分析生物标志物的多种代谢途径，获得差异代谢物的富集分析和生物学功能。

2.6 统计分析

数据以平均值±标准差 (mean ± SD) 表示。采用 Graph Pad Prism (version 9.0, GraphPad, USA) 软件进行组间单因素方差分析。以* $p < 0.05$ 为差异有统计学意义。

3.结果

3.1 连栀矾溶液对 UC 大鼠的治疗作用

本研究采用 TNBS 灌肠的方式进行 UC 大鼠的造模，通过对 UC 大鼠的体重变化、DAI 评分以及结肠长度等常规治疗指标进行记录，初步评价连栀矾溶液对 UC 的治疗效果。

3.1.1 大鼠体重变化

体重变化结果如图 3-1 所示，对照组大鼠的体重随着时间的变化有所上涨（约 7%），而 TNBS 诱导的模型组大鼠体重明显下降(第 7 天下降了约 16%， $p < 0.05$)。而经 LZF 溶液治疗后明显缓解了大鼠体重下降的趋势，与连栀矾溶液低剂量组 (LZF-L) 治疗组相比，连栀矾溶液高剂量组 (LZF-H) 抑制 TNBS 诱导的 UC 大鼠体重下降效果最为明显，与模型组有显著性差异。

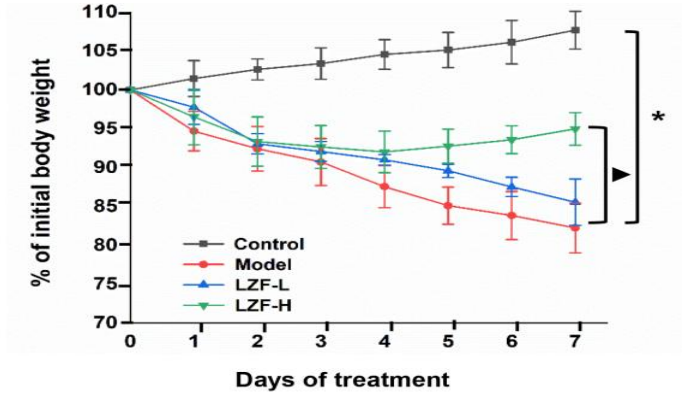


图 3-1.不同分组大鼠的体重变化图

Figure 3-1. Graph of the body weight of rats after oral administration of different concentration of LZF solution over time.

3.1.2 DAI 评分

不同分组的疾病活动指数（DAI）评分图如图 3-2 所示，对照组的大鼠在整个实验过程中没有表现出腹泻、便血等情况，其 DAI 评分结果较为稳定。而其余各组的 DAI 评分与对照组相比均存在差异，其中模型组 DAI 评分持续在 8~10 分。而在第 4 天到第 7 天，经连翘砒溶液治疗后大鼠的 DAI 评分有所下降，且与连翘砒溶液低剂量组（LZF-L）相比，连翘砒溶液高剂量组（LZF-H）治疗效果最为显著，与模型组具有显著性差异（ $p < 0.05$ ）。

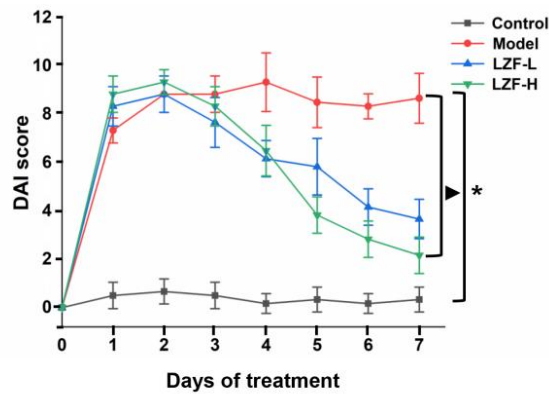


图 3-2 不同分组大鼠的 DAI 评分图

Figure 3-2 Graphs of DAI score in different groups

3.1.3 大鼠结肠长度变化

图 3-3 为各组大鼠的结肠长度图。结果显示，与对照组相比，模型组大鼠的结肠长度明显缩短 ($p < 0.05$)，且结肠组织水肿，粪便血迹明显，表明大鼠使用 TNBS 造模成功。如图中 B 所示，与对照组相比，模型组大鼠的结肠缩短了约 5 cm，而经过不同浓度的连翘酚溶液治疗后，结肠缩短现象有所改善，其中连翘酚溶液高剂量组 (LZF-H) 效果最为显著 ($p < 0.05$)。

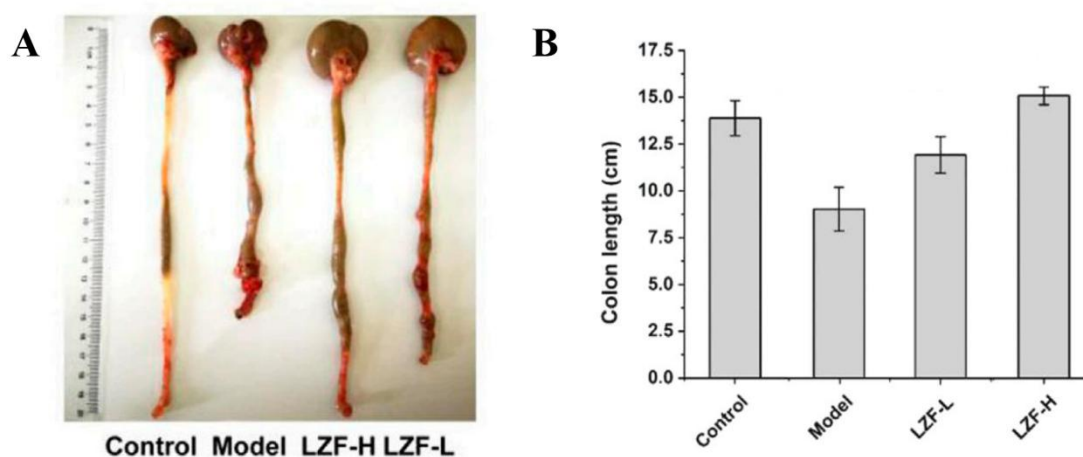


图 3-3 A.不同分组大鼠的结肠图; B.不同分组大鼠的结肠长度图

Figure 3-3 A. Images of colon in different groups; B. Graph of colon length in different groups.

总之，结肠炎症的相关评价指标，包括结肠长度、体重变化以及 DAI 评分的结果均显示连翘酚溶液能显著改善 TNBS 诱导的 UC 症状，且治疗效果随剂量增加而增强。

3.2 结肠组织切片 HE 染色结果

采用 HE 染色切片，通过比较形态和大小观察结肠组织中炎性细胞的浸润情况，从而反映结肠组织的炎性缺失情况^[74]。组织切片结果显示 (图 3-4)，正常组大鼠结肠组织结构清晰，肠黏膜结构完整，肠隐窝排列整齐，杯状细胞丰富，黏膜下层无充血水肿及糜烂。与正常组相比，模型组大鼠结肠组织结构破坏，可见不同程度

的肠黏膜脱落，腺体形状不规则，排列散乱，伴有隐窝脓肿，同时存在大量炎性细胞浸润，并具有较多溃疡及糜烂点；连梳矾溶液低剂量组（LZF-L）大鼠结肠黏膜周围上皮增收修复，未见明显缺损，相比于模型组其粘膜脱落程度降低，隐窝结构保持完整，但黏膜下层有炎性细胞浸润及明显水肿；连梳矾溶液高剂量组（LZF-H）大鼠结肠黏膜组织少量脱落，隐窝结构完整，杯状细胞丰富，黏膜下层无水肿。连梳矾溶液低剂量组的 HE 染色结果与连梳矾溶液高剂量组（LZF-H）相比，整体病理特征水平较为严重，可见大鼠结肠黏膜脱落程度较高，黏膜下层炎性细胞浸润严重且有水肿。以上结果表明，TNBS 溶液诱导的大鼠结肠炎造模成功，且连梳矾溶液对 TNBS 溶液诱导的大鼠结肠炎具有一定的改善作用，可以改善其结肠病理组织结构，其中连梳矾溶液高剂量组（LZF-H）的改善效果明显优于低剂量组（LZF-L），表明其治疗效果随着剂量的增加而增强。

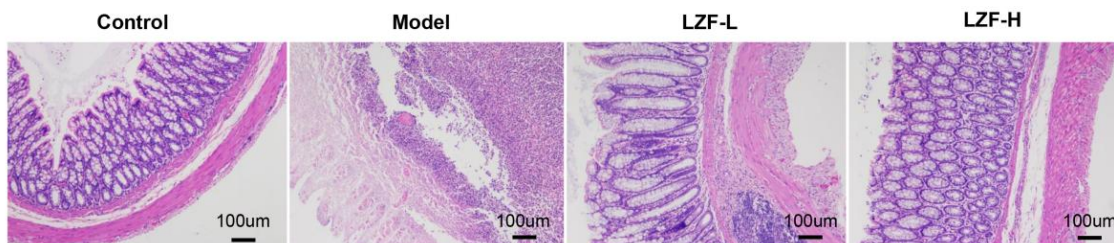


图 3-4 不同分组大鼠的结肠组织病理切片

Fig.3-4 Histopathological section of colon in different groups

3.3 HPLC-Q-TOF-MS 数据的多变量分析

采用 HPLC-Q-TOF-MS 在正、负离子模式下获得各组血清样品的质谱信息，为了寻找 4 组之间的直观差异，将归一化、保留时间校正和峰提取后的多维数据导入 SIMCA 14.0 软件进行多元统计分析。血清代谢轮廓的概述最初是通过 PLS-DA 分析进行，获得了理想的组间分离，并提高了对分类变量的识别。

为了判断模型的可靠性和准确性，提供了 PLS-DA 得分图和 200X 置换检验方法进行评价，见图 3-5 A~D；在负离子模式下（图 3-5 D）， $R_2X = 0.447$ ， $R_2Y = 0.911$ ，

$Q_2 = 0.601$ ，表明模型未发生过拟合。PLS-DA 分析表明，在正、负离子模式下，对照组、模型组、连梳砷溶液低剂量组（LZF-L）和连梳砷溶液高剂量组（LZF-H）之间的血清样品表现出明显不同的分类和分离。连梳砷溶液低剂量组（LZF-L）、连梳砷溶液高剂量组（LZF-H）较模型组逐渐接近正常组，可认为 TNBS 诱导的 UC 模型成功。因此，这些结果表明各组血清样品分离度良好，有利于进一步筛选差异代谢物。

为了进一步寻找两组之间的差异代谢物，采用 OPLS-DA 在正、负离子模式下分别对对照组与模型组、模型与连梳砷溶液低剂量组（LZF-L）、模型与连梳砷溶液高剂量组（LZF-H）进行了较好的区分。根据变量投影重要性（VIP）值（ $VIP > 1$ ），代谢物 VIP 值越高，表明这些变量对各组分离的贡献越大。结果表明 OPLS-DA 模型具有良好的拟合度和预测能力。

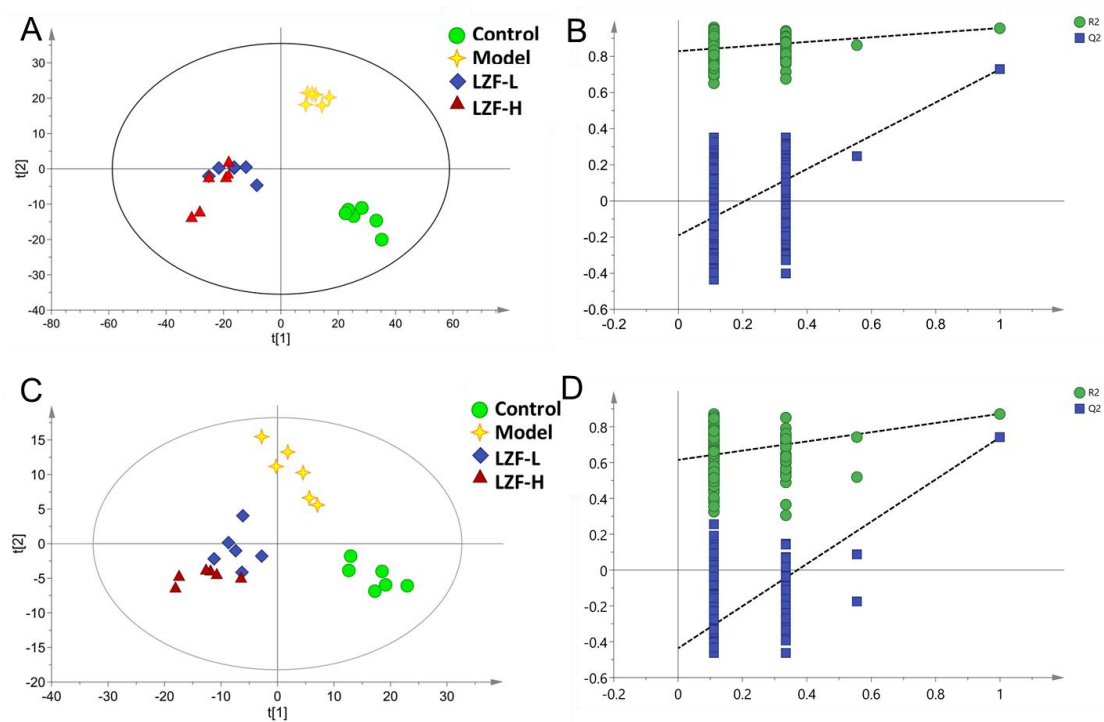


图 3-5 血清质谱数据的多元统计分析

A.正离子模式下 PLS - DA 得分图; B.负离子模式下 PLS - DA 得分图; C.正离子模式下 PLS - DA 得分图的 200 次置换检验; D.负离子模式下 PLS - DA 得分图的 200 次置换检验

Fig. 3-5 Multivariate statistical analysis of serum mass spectrometry data

A. PLS-DA score plot in positive ion mode; B. PLS-DA score plot in negative ion mode; C. 200 permutation tests of the PLS-DA score plot in positive ion mode; D. 200 permutation tests of the PLS-DA score plot in negative ion mode

3.4 差异生物标志物的结构鉴定

根据以上各组样本 OPLS-DA 的 VIP 得分，结合 SPSS 软件进行单因素方差分析检验，当满足 $VIP \geq 1$ 且 $p \leq 0.05$ 时，筛选出的离子作为潜在生物标志物。选取 VIP 值较高的 35 个代谢物离子，从血清样品中分离，用于进一步研究。通过基于精确分子质量测量、碎片离子、质谱峰数据和分子式的单因素方差分析检验，最终只有 14 个被确定为对照组和 TNBS 溶液处理组大鼠的潜在生物标志物，见表 3-3，包括氨基酸、胆汁酸、脂肪酸、多肽、维生素等。

而模型组与正常组相比上调或下调时连枢矾溶液治疗组会倾向于向正常组回调。最后，采用 One Way ANOVA 检验分析这些差异代谢物的变化趋势，并用 FDR 方法进行校正，以 4 组峰面积绘制的统计直方图如图 3-6 所示。

进一步结合相关性分析热图蓝色表示负相关，红色表示正相关，颜色深浅表示相关，模型组与低剂量组之间差异代谢物生物标志物的变化趋势见图 3-7。含肌酸（Creatine）、烟酰胺（Niacinamide）、泛酸（Pantothenic acid）、Leucylproline 和 8-HETE 的 5 种代谢物在模型组中呈升高趋势，其他代谢物在低剂量组中呈降低趋势。这些结果与上述结果一致。

表 3-3 确定溃疡性结肠炎的潜在生物标志物

Table.3-3 Identified potential biomarkers of ulcerative colitis

No.	Metabolites	Rt (min)	Determined mass (m/z)	Calculated mass (m/z)	Mass error (ppm)	Formula	Ion mode	VIP value	q value
1	L-Valine	0.86	140.0681	140.0682	1	C ₅ H ₁₁ NO ₂	[M+Na] ⁺	4.05	<0.0001
2	Creatine	0.88	132.0772	132.0768	3	C ₄ H ₉ N ₃ O ₂	[M+H] ⁺	2.15	0.0059
3	L-Alanine	0.88	90.0557	90.0550	8	C ₃ H ₇ NO ₂	[M+H] ⁺	2.56	0.0018
4	Niacinamide	1.07	123.0554	123.0553	1	C ₆ H ₆ N ₂ O	[M+H] ⁺	1.75	0.0012
5	Leucylproline	1.50	229.1552	229.1547	2	C ₁₁ H ₂₀ N ₂ O ₃	[M+H] ⁺	3.35	0.0004
6	Pantothenic acid	2.09	220.1164	220.1179	7	C ₉ H ₁₇ NO ₅	[M+H] ⁺	2.49	0.0156
7	Cholic acid	8.13	407.2768	407.2803	9	C ₂₄ H ₄₀ O ₅	[M-H] ⁻	2.08	0.0237
8	LysoPC(16:1)	9.06	494.3224	494.3241	3	C ₂₄ H ₄₈ NO ₇ P	[M+H] ⁺	3.22	0.0471
9	Taurocholic acid	9.06	516.3033	516.2989	8	C ₂₆ H ₄₅ NO ₇ S	[M+H] ⁺	1.78	0.0078
10	LysoPC(15:0)	9.25	482.3217	482.3241	5	C ₂₃ H ₄₈ NO ₇ P	[M+H] ⁺	3.26	0.0011
11	LysoPE(18:0)	9.25	526.3118	526.3150	6	C ₂₃ H ₄₈ NO ₇ P	[M+FA-H] -	1.41	<0.0001
12	8-HETE	9.95	319.2247	319.2279	10	C ₂₀ H ₃₂ O ₃	[M-H] ⁻	3.64	0.0262
13	LysoPE(20:1)	10.05	506.3218	506.3252	7	C ₂₅ H ₅₀ NO ₇ P	[M-H] ⁻	1.07	0.0038
14	Docosapentaenoic acid (22n-3)	13.62	329.2472	329.2486	4	C ₂₂ H ₃₄ O ₂	[M-H] ⁻	1.12	0.0311

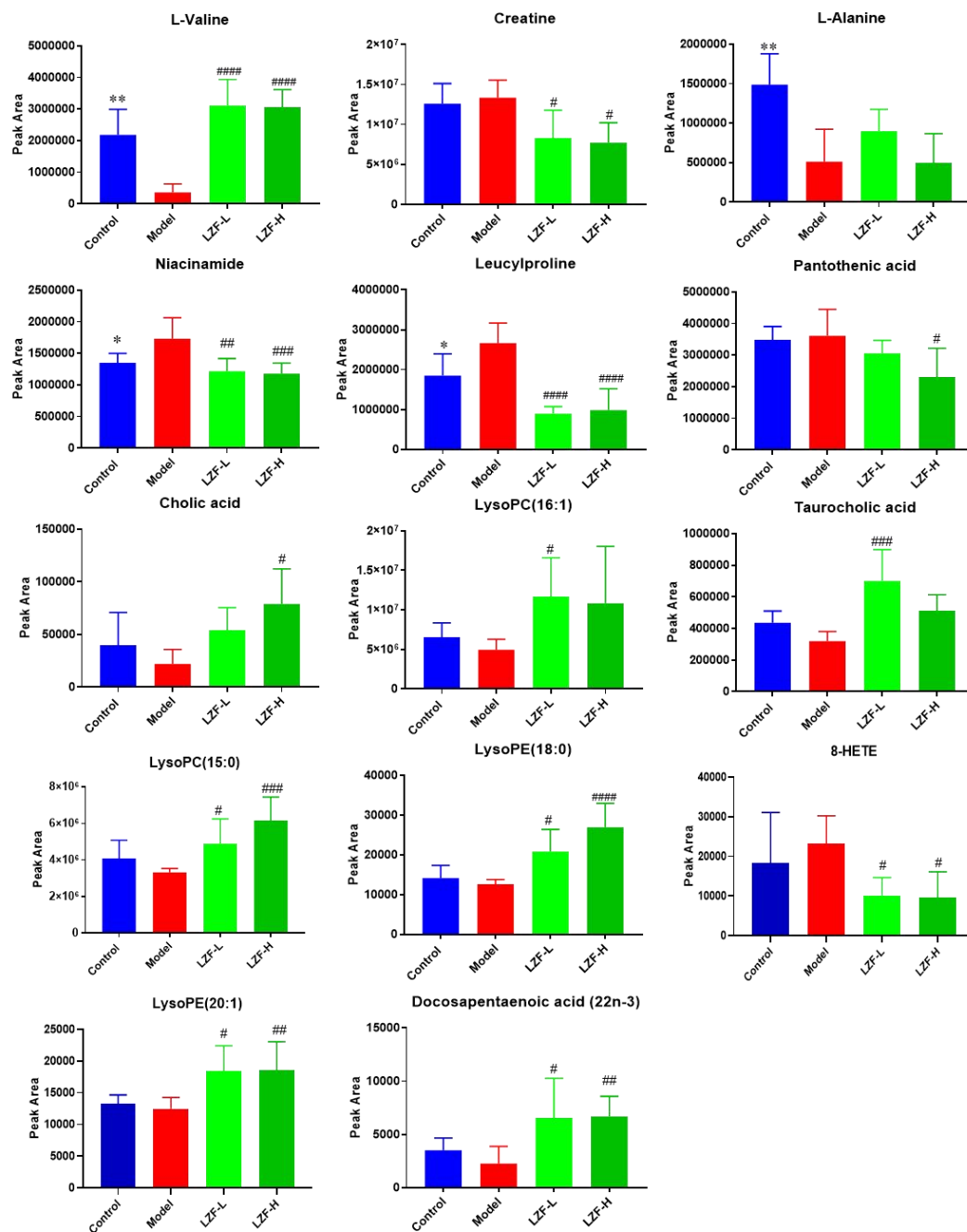


图 3-6 14 个差异代谢物(* $p < 0.05$, ** $p < 0.01$, *** $p < 0.001$, 对照组 vs 模型对照组; # $p < 0.05$, ## $p < 0.01$, ### $p < 0.001$ 低剂量, 连翘矾溶液组 vs 模型对照组)的峰面积分析

Fig.3-6 Peak area analysis of 14 differential metabolites (* $p < 0.05$, ** $p < 0.01$, *** $p < 0.001$, control group vs model control; # $p < 0.05$, ## $p < 0.01$, ### $p < 0.001$ low-dose, LZF solution group vs model control)

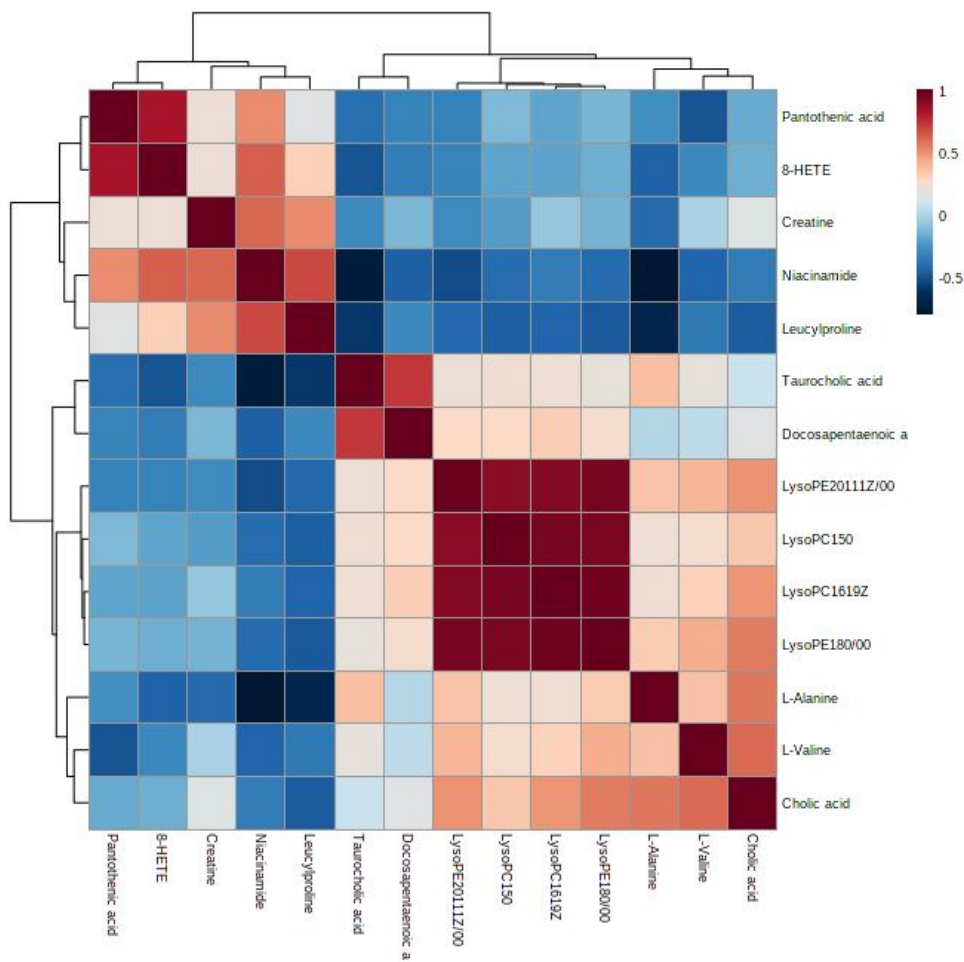


图 3-7 .低剂量组与模型组相比潜在代谢物生物标志物的相关性分析

Fig 3-7. The correlation analysis of potential metabolites biomarkers in the low-dose group compared to the model group

3.5 不同 ROC 曲线的诊断价值分析

表征潜在代谢组学生物标志物的临床诊断价值是一项主要任务，利用接受者操作特性曲线（receiver operating characteristic, ROC）曲线评估生物标志物在两组间的诊断准确性已在许多研究中取得成功。ROC 曲线下面积（area under the curve, AUC）用于评估临床价值，AUC 值大于 0.8 的生物标志物具有较高的准确性和明显的差异性。如图 3-8 所示，AUC 值 > 0.8，诊断敏感性和特异性均较高，表明这些代谢物作为 TNBS 诱导 UC 疾病诊断的生物标志物具有较高的临床诊断价值。其中，

L-丙氨酸 (AUC = 1.000)、牛磺胆酸 (AUC = 0.917)、烟酰胺 (AUC = 0.861)、胆酸 (AUC = 0.861)、L-缬氨酸 (AUC = 0.847) 的 AUC > 0.8, 有效辅助 TNBS 诱导的 UC 疾病诊断。

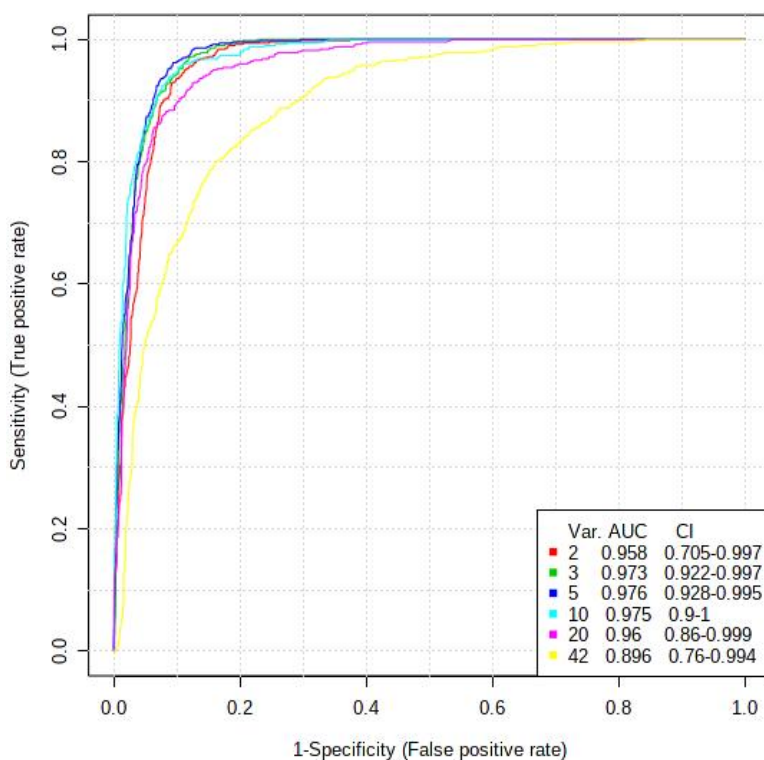


图 3-8 对照组与模型组之间 14 种潜在生物标志物的 ROC 曲线分析

Fig 3-8 ROC curve analysis of 14 potential biomarkers between control group and model group

3.6 代谢通路分析

将 14 个差异代谢物导入 MetaboAnalyst 5.0 以探索连栀矾溶液抗 UC 的潜在机制。发现差异生物标志物主要影响 12 条代谢通路。连栀矾溶液主要影响其中 5 条通路, 即烟酸和烟酰胺代谢、精氨酸和脯氨酸代谢、初级胆汁酸生物合成、甘油磷脂代谢、泛酸和辅酶 A 生物合成, 见图 3-9 和表 3-4, 上述通路可能是连栀矾溶液处

理后内源性物质代谢变化的潜在机制。基于 KEGG 数据库，对代谢通路进行分析，形成潜在的代谢通路网络图（图 3-10）。可见连梳矾溶液不仅影响单一的代谢通路，而且通过相互关联的代谢通路形成复杂的代谢通路网络，从而达到治疗 UC 的目的。

此外，体内多种代谢途径相互关联，药物通过多途径发挥协同作用。因此，构建代谢通路互连网络有利于描述连梳矾溶液对 UC 大鼠的治疗机制。如图 3-13 所示，不同代谢通路的相互作用表明 UC 是一种涉及多种代谢紊乱的疾病，通过调节氨基酸代谢、脂肪代谢和能量生成，而连梳矾溶液通过调节这些代谢通路改善 UC。

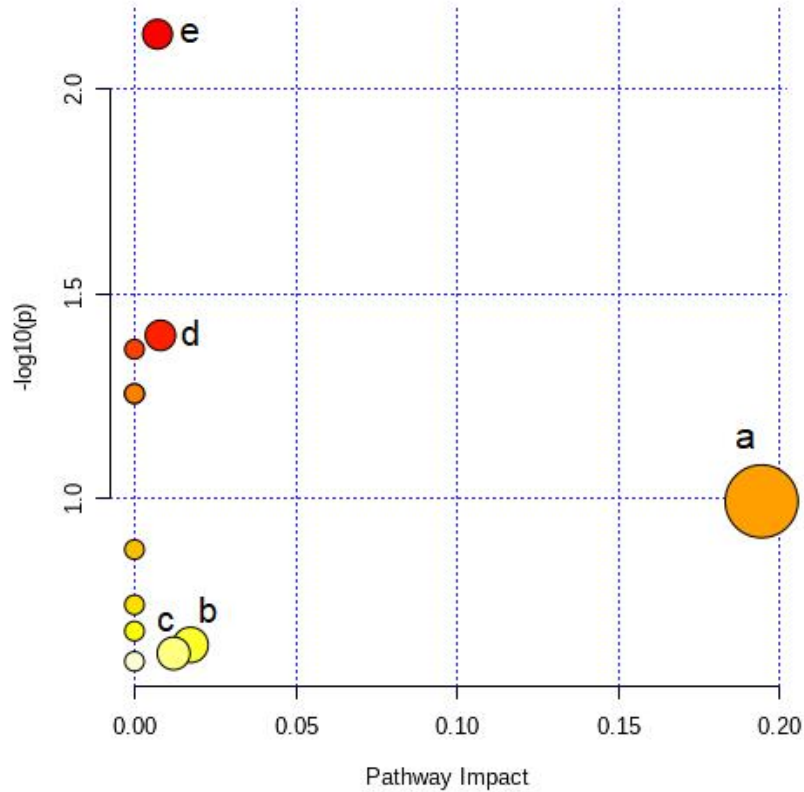


图 3-9 代谢通路分析影响值

Fig.3-9 Impact value of metabolic pathway analysis

表 3-4 潜在生物标志物的代谢通路总结

Table. 3-4 Summary of metabolic pathways of potential biomarkers

Metabolic pathways	Total	Hits	Raw p	-log(p)	Impact	No. in Fig.6
Pantothenate and CoA biosynthesis	19	2	0.0073339	2.1347	0.00714	e
Primary bile acid biosynthesis	46	2	0.039973	1.3982	0.00805	d
Aminoacyl-tRNA biosynthesis	48	2	0.043228	1.3642	0	-
Valine, leucine and isoleucine biosynthesis	8	1	0.055506	1.2557	0	-
Taurine and hypotaurine metabolism	8	1	0.055506	1.2557	0	-
Nicotinate and nicotinamide metabolism	15	1	0.10176	0.99242	0.1943	a
Selenocompound metabolism	20	1	0.13353	0.87443	0	-
Alanine, aspartate and glutamate metabolism	28	1	0.18224	0.73936	0	-
Glycine, serine and threonine metabolism	33	1	0.2114	0.67489	0	-
Glycerophospholipid metabolism	36	1	0.22844	0.64122	0.01736	b
Arginine and proline metabolism	38	1	0.23962	0.62048	0.01212	c
Valine, leucine and isoleucine degradation	40	1	0.25064	0.60094	0	-

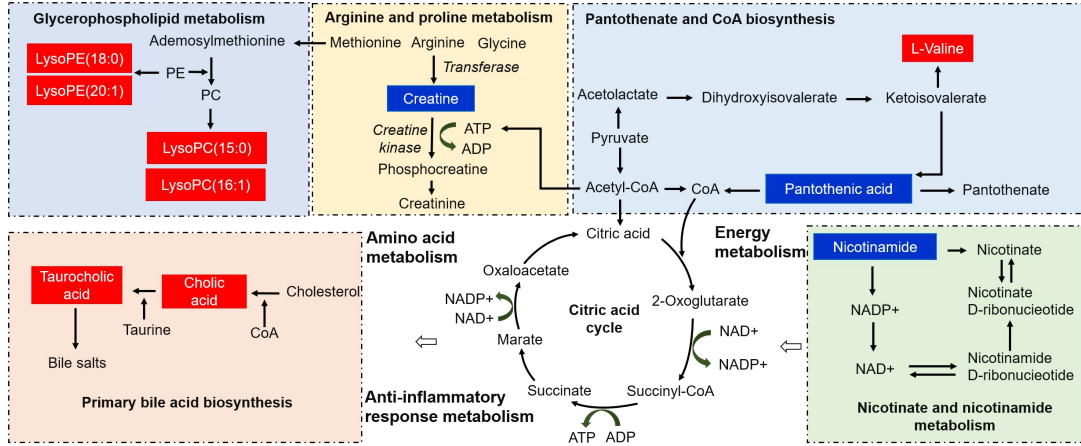


图 3-10 连梳矾溶液治疗 TNBS 诱导 UC 的相关通路网络

红色和蓝色分别代表代谢物含量较模型组增加和减少。（PC：磷脂酰胆碱，PE：磷脂酰乙醇胺，Lyso PC：溶血磷脂酰胆碱，Lyso PE：溶血磷脂酰乙醇胺）

Fig.3-10 Correlation pathway networks of treatment of LZF solution to TNBS-induced UC

The red and blue respectively represent the content of metabolites increase and decrease compared with model group. (PC: Phosphatidylcholine, PE: Phosphatidylethanolamine, LysoPC: Lysophosphatidylcholine, LysoPE: Lyso Phosphatidylethanolamine)

4.小结与讨论

4.1 小结

本部分采用连梳矾溶液，进一步探究其改善大鼠结直肠炎（保留灌肠）的药效作用。结果表明连梳矾溶液表现出抗结直肠炎（保留灌肠）作用，能显著抑制 TNBS 诱导的大鼠体重下降、DAI 评分升高、结肠缩短及肠组织炎性浸润等疾病特征，且作用呈剂量依赖性。大鼠结肠组织 HE 染色结果表明，连梳矾溶液可以显著改善 TNBS 溶液诱导的结肠炎大鼠的结肠组织病理情况，且随剂量的提升效果增强，给药后大鼠结肠组织较模型组，黏膜层脱落程度明显降低，炎性细胞浸润情况明显得到改善，杯状细胞增多，且连梳矾溶液高剂量组较连梳矾溶液低剂量组病理情况更趋近于正常组。

基于非靶向血清代谢组学技术，从内源性代谢物的角度，分析大鼠结直肠炎（保留灌肠）在连梳矾溶液治疗后血清代谢物的变化规律，寻找标志性内源性代谢物和

代谢通路，以探讨连梳砒溶液治疗结直肠炎（保留灌肠）的分子作用机制。并进行 PCA、PLS-DA、OPLS-DA 多元统计分析，发现无论是正离子模式还是负离子模式，正常组与模型组均能很好地区分，说明模型建立成功，同时连梳砒溶液组与模型组也能完全分离，且更趋近于正常组。根据 VIP 值 (>1.5) 和 T 检验 ($p < 0.05$) 共筛选出 14 个差异代谢物，与正常组相比，模型组大鼠血清中 5 个差异代谢物（肌酸（Creatine）、烟酰胺（Niacinamide）、泛酸（Pantothenic acid）、Leucylproline 和 8-HETE）呈显著升高的趋势，其他代谢物在低剂量组中呈降低趋势。用连梳砒溶液治疗后，5 个差异代谢物（肌酸（Creatine）、烟酰胺（Niacinamide）、泛酸（Pantothenic acid）、Leucylproline 和 8-HETE）趋于恢复正常水平，说明连梳砒溶液可以在一定程度上调节 UC 大鼠的代谢紊乱。代谢通路分析结果表明，这 14 个标志性代谢物主要影响 12 条代谢通路，连梳砒溶液主要影响其中五条通路，即烟酸和烟酰胺代谢、甘油磷脂代谢、精氨酸和脯氨酸代谢、初级胆汁酸生物合成、泛酸和辅酶 A 生物合成，上述通路可能是连梳砒溶液处理后内源性物质代谢变化的潜在机制。基于 KEGG 数据库，对代谢通路进行分析，形成潜在的代谢通路网络图。可见连梳砒溶液不仅影响单一的代谢通路，而且通过相互关联的代谢通路形成复杂的代谢通路网络，从而达到治疗结直肠炎（保留灌肠）的目的。因此，连梳砒溶液通过调节氨基酸代谢、脂肪代谢和能量生成改善结直肠炎（保留灌肠）。

4.2 讨论

本研究采用高通量 HPLC-QTOF-MS 方法证明了连梳砒溶液对结直肠炎（保留灌肠）大鼠的作用机制。共鉴定出 14 种潜在生物标志物，包括氨基酸、胆汁酸、脂质种类、多肽和维生素等。

连梳砒溶液通过调节泛酸和 CoA 生物合成 (Pantothenate and CoA biosynthesis)、烟酸和烟酰胺代谢 (Nicotinate and nicotinamide metabolism)、初级胆汁酸生物合成 (Primary bile acid biosynthesis)、甘油磷脂代谢 (Glycerophospholipid metabolism)、精氨酸和脯氨酸代谢 (Arginine and proline metabolism) 等 5 条重要的代谢途径，在调节能量生成、氨基酸、抗炎代谢紊乱方面发挥关键作用。下面对上述潜在分子的生物学意义和优势通路进行讨论，进一步揭示连梳砒溶液对结直肠炎（保留灌肠）

大鼠的作用机制。

能量代谢是为所有代谢活动提供能量的最基本的有机方式。连梳矾溶液治疗结肠炎（保留灌肠）大鼠主要包括泛酸和辅酶 A 生物合成、烟酸和烟酰胺代谢两条能量代谢途径。泛酸和 L-缬氨酸均参与泛酸和辅酶 A 生物合成的能量调控途径。泛酸是一种 B5 维生素，通过合成辅酶 A（COA）参与许多代谢反应，为机体提供能量^[75]。

研究表明结肠炎患者结肠细胞能量产生减少，病变黏膜中结合态泛酸向辅酶 A 的转化受阻，导致溃疡性结肠炎相关血清中泛酸水平升高。L-缬氨酸也是与泛酸协同调控泛酸和辅酶 A 生物合成途径的必需氨基酸。

采用最佳体外抗炎组分即发酵后的连梳矾溶液，建立 2,4,6-三硝基苯磺酸（2,4,6-trinitrobenzenesulfonic acid, TNBS）诱导的溃疡性结肠炎（UC）大鼠模型，在 UC 大鼠模型治疗过程中，抗炎代谢通路也发生了改变，包括甘油磷脂代谢和初级胆汁酸生物合成。胆酸(cholic acid, CA)是肝脏中胆固醇首先催化生成的初级胆汁酸(primary bile acids, BAs)，可促进膳食脂质和脂溶性维生素 A、D、E、K 进入肠道消化吸收。然后 CA 通过 CoA 合成酶与牛磺酸结合形成牛磺胆酸(taurocholic acid, TCA)。大约 5 %的胆汁酸逃逸到结肠，肠道共生菌通过法尼醇 X 受体(farnesoid X receptor, FXR)、维生素 D 受体(vitamin D receptor, VDR)、孕烷 X 受体(pregnenolone X receptor, PXR)和 G 蛋白偶联受体(G protein-coupled receptor, TGR5)^[76,77]等核受体将胆汁酸转化为多种肠道次级胆汁酸，这些次级胆汁酸是调节胆固醇代谢、能量平衡、肠道运动和细菌生长以及炎症的关键激素。

研究中，由于 TNBS 诱导的 UC 疾病中 ATP 供能不足，模型组肌酸水平低于对照组。由此推断，组织对肌酸的摄取会受阻，导致含量和积累增加，进而影响精氨酸和脯氨酸代谢的紊乱。而连梳矾溶液治疗改善了改变的代谢物和通路来修复结肠屏障功能，Creatine 被正常的能量代谢功能下调，细胞内 CoA 水平升高，ATP 合成增加。这些结果表明，含肌酸的氨基酸代谢在结肠炎（保留灌肠）疾病中发挥着重要的生物学作用，通过抑制炎症、减少氧化应激，直接或间接地将能量代谢与肠道稳态联系起来。